Chapter 2

Leaf Energy Balance: Basics, and Modeling from Leaves to Canopies

Vincent P. Gutschick*
Global Change Consulting Consortium, Inc., Las Cruces, NM 88011, USA

*Author for correspondence, e-mail: vinceg@gcconsortium.com
http://gcconsortium.com

K. Hikosaka, Ü. Niinemets, and N.P.R. Anten (eds.), *Canopy Photosynthesis: From Basics to Applications*, DOI 10.1007/978-94-017-7291-4_2

Summary

An initial review of diverse studies from leaf to globe clarifies the importance of accurate modeling of leaf temperature. The body of the discussion here then shows that the tools for modeling exist at diverse levels of process detail. Modelers are able to assemble a workable toolkit from the whole set of such tools. I present explicit equations for leaves in isolation and in canopies. Toward enabling comprehensive process-based modeling, I discuss energy-balance modeling in the forward direction for prediction of photosynthesis, transpiration, and other measures, including collateral effects such as leaf damage from excess temperatures. Included here are several useful mathematical solution methods for highly-coupled processes, such as energy balance, photosynthesis, stomatal control, and scalar transport. I review inverse modeling to estimate evapotranspiration and plant water stress from measured leaf temperatures. Quantitative arguments indicate the range and limits of validity of various approximations, such as ignoring lateral heat

Symbols: A – Leaf photosynthetic rate per area [μmol m^{-2} s^{-1}]; A_{LL} – Light-limited A [μmol m^{-2} s^{-1}]; A_{sat} – Light-saturated A [μmol m^{-2} s^{-1}]; a_{NIR} – Absorptance of leaves in the NIR [-]; a_{PAR} – Absorptance of leaves in the PAR [-]; b_{BB} – Residual stomatal conductance in Ball-Berry equation [mol m^{-2} s^{-1}]; b_c, b_E, b_{TIR} – Derivative of energy-balance terms with respect to temperature [W m^{-2} K^{-1}]; B – Sum of the derivatives of the energy-balance terms [W m^{-2} K^{-1}]; C_a, C_c, C_i, C_s – Partial pressure of CO_2 in ambient air, at the chloroplast, in the leaf interior (substomatal cavities), at the leaf surface beneath the boundary layer [Pa]; $C_{P,m}$ – (Molar) heat capacity of air [J mol^{-1} K^{-1}]; $C_{P,a}$ – Leaf heat capacity per unit area [J m^{-2} K^{-1}]; d – Zero-plane displacement height in a canopy [m]; d_{leaf} – Characteristic linear dimension of a leaf for heat transfer (m); E_{leaf} – Leaf transpiration rate [mol m^{-2} s^{-1}]; e_a, e_i, e_s – Partial pressure of water vapor in ambient air, in the leaf interior (substomatal chamber), at the leaf surface beneath the boundary layer [Pa]; e_{sat} – Saturated water vapor pressure [Pa]; E_{NIR}, E_{PAR}, E_{TIR} – Energy flux density in the NIR, PAR, TIR [W m^{-2}]; ET – Evapotranspiration rate [various units, including mm d^{-1}]; G – Soil heat flux density [W m^{-2}]; g_{aH} – Canopy aerodynamic conductance for heat [preferred as mol m^{-2} s^{-1}]; g_b, g_b' – Leaf boundary-layer conductance for water vapor, CO_2 [mol m^{-2} s^{-1}]; g_{bh} – Boundary-layer conductance for heat [preferred as mol m^{-2} s^{-1}]; g_{bs}, g_{bs}' – Combined boundary-layer and stomatal conductance of leaves for water vapor, CO_2 [mol m^{-2} s^{-1}]; g_s, g_s' – Stomatal conductance for water vapor, CO_2 [mol m^{-2} s^{-1}]; h – Canopy height [m]; h_s – Relative humidity at the leaf surface, beneath the boundary layer [-]; H – Sensible heat flux density (leaf or canopy) [W m^{-2}]; k – von Karman's constant [-]; K_{CO} – Effective Michaelis constant for CO_2 binding to Rubisco [Pa]; K_H, K_w, K_{CO_2} – Eddy diffusivity for heat, water vapor CO_2 [m^2 s^{-1}]; LE – Latent heat flux density [W m^{-2}]; m_{BB} – Slope in the Ball-Berry equation for stomatal conductance [-]; P_a – Total air pressure [Pa]; *NIR* – Near-infrared radiation (700–2500 nm); *PAR* – Photosynthetically active radiation (400–700 nm); *PPFD* – Photosynthetic photon flux density [mol m^{-2} s^{-1}]; Q – Generic heat flux density [W m^{-2}]; Q_c^-, Q_E^- – Flux density of heat loss from convection, transpiration [W m^{-2}]; Q_{SW}^+, Q_{TIR}^+ – Flux density of energy gain from shortwave, TIR absorption [W m^{-2}]; Q_{TIR}^- – Flux density of energy loss from TIR emission [W m^{-2}]; R_d – Dark respiration rate per leaf area [μmol m^{-2} s^{-1}]; R_n – Net radiation flux density [W m^{-2}]; T – Temperature [°C or K, as appropriate]; T_{air} – Air temperature [°C or K, as appropriate]; T_{leaf} – Leaf temperature [°C]; T_{mean} – Mean temperature to which dark respiration acclimates [°C]; *TIR* – Thermal infared radiation (2.5–15 μm, long-wave radiation); u – Wind speed [m s^{-1}]; u_* – Friction velocity [m s^{-1}]; $V_{c,\max}$ – Maximal carboxylation capacity per leaf area [μmol m^{-2} s^{-1}]; z – Height above the soil [m]; z_H, z_m – Roughness lengths for heat transport, momentum [m]; ΔT – Shift in leaf temperature as transient [°C or K]; δ – Small nominal change in incoming shortwave solar energy flux density [W m^{-2}]; $\Gamma*$ – Compensation partial pressure of CO_2 in photosynthesis without dark respiration [Pa]; ε, $\varepsilon_{sky,eff}$ – Thermal emissivity of leaf, sky [-]; ς – Atmospheric stability measure [-]; θ – Transition parameter between light-limited and light-saturated photosynthetic rates [-]; λ – Latent heat of vaporization of water [preferred as J mol^{-1}]; ρ – Molar density of air [mol m^{-3}]; σ – Stefan-Boltzmann constant [W m^{-2} K^{-4}]; φ – Initial quantum yield of photosynthesis [mol CO_2 (mol photons)$^{-1}$]; ψ_{leaf} – Leaf water potential [MPa]; ψ_H, ψ_m – Atmospheric stability corrections for heat, momentum transfer [-]

conduction in the leaf lamina or, on certain time-scales, transients in leaf temperature. Overall, the review emphasizes the importance of including the energy balance in models and provides suggestions for making practical error estimates of process-model inaccuracies and process incompleteness. The current limitations compel the development of improved models.

Keywords Temperature • Energy balance • Leaves • Modeling • Radiation • Convection • Stomatal conductance • Transpiration • Canopies • Transients • Turbulent transport • Inverse modeling

I. Introduction: Why Leaf Energy Balance is Important to Model

Leaves cover approximately half of the land surface of the Earth at any one time (Myneni et al. 2002). They are correspondingly critical surfaces on land for the exchange of radiation and momentum and for scalar fluxes of heat, water vapor, CO_2, and other atmospheric constituents. Transpiration from leaves accounts for approximately half of total water emission from land surfaces (Lawrence et al. 2006), with simple evaporation (or sublimation of ice, snow) from soil accounting for the remainder. Leaves are key determinants of the carbon and water cycles and of climatic processes. Additionally, their trace gas emissions of terpenes and other volatile "secondary" metabolic compounds are important in atmospheric chemistry (e.g., Räisänen et al. 2009) and in contributing condensation nuclei for the formation of clouds (Kavouras et al. 1998; Hartz et al. 2005). The emission of both isoprene and terpenes is heavily dependent upon leaf temperature (Peñuelas and Llusià 2003; Monson et al. 2012; Grote et al. 2013).

Leaf energy balance (total or gross energy balance) determines leaf temperature. In turn, leaf temperature conditions affect numerous physiological processes as well as climatic processes. Physiologically, leaf temperature sets the activation of biochemical processes, particularly photosynthesis and respiration (Chap. 3, Hikosaka et al. 2016a), as one sees incorporated in all current models of leaf photosynthesis, largely based on the seminal model of Farquhar et al. (1980). By extension, leaf temperature can also generate deactivation, directly via enzyme deactivation, commonly at high temperatures but also at low temperatures, particularly for C_4 plants, whose PEP carboxylase enzyme deactivates or even falls apart reversibly at low temperatures (Kleczkowski and Edwards 1991; Sage and Kubien 2007). Temperature extremes also may generate photoinhibition of photosynthetic quantum yields or capacity over short to long duration (Ball et al. 2002; Demmig-Adams and Adams 2006), when high fluxes of absorbed photosynthetic photon flux density, or PPFD, cannot be driven productively into photosynthetic photochemistry nor dumped by radiationless relaxation of the xanthophyll pigments. Leaf temperature also acts with genetic programs in determining plant development; the empirical degree-day model has been verified at scales ranging from molecular to whole plant (Granier et al. 2000). At the level of the plant, leaf temperature is also an important factor in the propagation of plant diseases, particularly fungal diseases (Schuepp 1993; Harvell et al. 2002).

Leaf energy balance includes the exchanges of sensible and latent heat with the air as well as radiative processes. Exchanges of sensible and latent heat with the atmosphere by leaves and soil (or other non-leafy surfaces) are the principal energy inputs to the atmosphere over land, balanced in the long term by thermal infra-red (TIR) emissions to space (Hartmann 1994). On diverse spatial scales, these exchanges generate convective air flows – free convection on single leaves (see Campbell and Norman 1998), up to mesoscale flows that may lead to cloud formation (Anthes 1984; Segal et al. 1988), and on to larger scales, ultimately global. Physiology re-enters the formulation of heat exchanges at leaves: photosynthesis, itself temperature-dependent, is tightly coupled to leaf stomatal conductance, g_s, as expressed in many empirical models of g_s (Ball et al. 1987; Dewar 2002; Leuning 1995). In turn, conductance is a factor in leaf transpiration (latent heat exchange) thereby affecting leaf temperature which ultimately couples back to photosynthesis. The need for coupled models of leaf energy balance, stomatal conductance, photosynthesis, and physical transport of heat and gases is apparent, as will be covered below. It may be surprising that, until 1986 (Verstraete and Dickinson 1986), climate models (general circulation models, or GCMs) did not consider leafed area on the globe as physiologically dynamic, rather they set a simple, uniform physical boundary condition for vegetated area. Now, the attention to the physiology of vegetated surfaces in GCMs is intense, and the role of vegetation in controlling temperature is well-recognized (e.g., Sellers et al. 1997).

An accurate knowledge of leaf temperature, whether by measurement or modeling or both, is necessary for comprehension and prediction of climate, including climate change. From a paleoclimatic perspective, understanding the relation of leaf temperature to climate is necessary to infer paleoclimate from tree rings. This is particularly true in attempting to use the stable isotopic composition (^{13}C, ^{2}H, ^{18}O) to infer climatic conditions – e.g., estimating past water stress via the relations among the $^{13}C/^{12}C$ ratio, the leaf's ratio of internal to external CO_2 partial pressures, water-use efficiency, and water stress (Barbour 2007).

The radiative portion of leaf energy balance merits attention on its own, for its effects on neighboring leaves and non-foliar surfaces that intercept scattered radiation from leaves and for total radiative interception on land (Chap. 1, Goudriaan 2016). Variably according to optical properties and orientation, leaves absorb and reflect at all major radiation wavebands: photosynthetically active (PAR, 400–700 nm), near infrared (NIR, 700–200 nm) and thermal infrared (TIR, 2.5–15 µm) radiations. Leaves also strongly absorb ultraviolet (UV) radiation, but it is a minor energy component. They also emit much TIR, as do all bodies. The transfers of radiation to and from leaves generate much of the complexity in models of leaf energy balance within canopies, given the vectorial rather than scalar nature of the propagation of radiation. Regarding the large-scale radiative balances, the deficit in absorption, or albedo, sets the overall availability of solar energy in the climate system. Recently the effect of leaf presence on regional albedo has received considerable attention in the discussion of climate (Hales et al. 2004) and of global warming (for a review see Bonan 2008). Afforestation at high latitudes is estimated to have a net warming effect, due to reduced surface albedo despite the ability of forests to take up CO_2 as a greenhouse gas (Bonan 2008).

All the process studies and modeling are an intellectual challenge in their own right and they also have much practical application. Understanding the components of leaf energy balance is needed in modeling crop productivity, whether for on-farm management or predictions of market conditions or famine warnings; in ecological studies of net primary production; in estimating water balance of landscapes, whether for irrigation management or predicting surface water balance for human use or ecosystem status; and, of course, in the climate modeling. Furthermore, inverse modeling of leaf temperature is also an important exercise (Box 2.1).

This review of the processes of energy balance and their consequences has diverse goals. It may impart to researchers with theoretical backgrounds but who are nonspecialists in biophysical modeling an appreciation of the various levels of phenomena. For researchers dealing with the biophysical phenomena but more focused on experimental approaches than a body of theory, it may aid in developing quantitative studies with the full power and accuracy of biophysical theory. For specialists attuned to biophysical theory, it may offer a more comprehensive view, such as by bringing attention to less-appreciated but important links of phenomena. One example is the importance of sky thermal infrared interception as a distinct energy input. Another example is providing justification for neglecting photosynthetic and thermal energy storage on most scales of space and time. Finally, for advanced students of botany, physiology, physics, and other disciplines who are in their early careers, this review is offered to give context to reading of the extensive literature related to leaf energy balance, and, one hopes, to generate fruitful research ideas.

Box 2.1 Inferring Water Stress and Water Use from Leaf Temperature

Measured leaf temperature can be used to infer water stress on plants, as in the classic crop water stress index of Idso et al. (1981) and in the numerous rectifications (Jackson et al. 1988) and extensions (Fuchs 1990), including in remote sensing (Kogan 1997). In related fashion, measured surface (leaf, soil) temperature can be used in estimating evapotranspiration (*ET*), a mass flux of water, a critical indicator of both plant productivity and surface water balance. One of the simpler effective models for this is the Surface Energy Balance Land (SEBAL) model, used in remote sensing (Bastiaanssen et al. 1998). The net radiative energy input, R_n, to the surface as an energy flux density is estimated from measured reflected fluxes and additional information (the solar constant, estimated atmospheric absorption, angle of solar illumination). The temperature difference from leaves to air is estimated from surface radiative temperature, invoking a calibration using hot ($ET = 0$) and cold (ET as maximal, sensible heat flux $H = 0$) extreme parts of the scene. Along with estimates of surface roughness, hence, of conductance for sensible heat, this allows for the estimation of H. Finally, one estimates latent heat energy flux density, $\lambda\ E$, as a residual, $\lambda\ E = R_n - G - H$. Here, E is the evapotranspiration rate written as a single-letter symbol, G is the flux into the soil, estimated empirically. More sophisticated process modeling is incorporated into allied inverse models that resolve leaf and soil temperatures (Li et al. 2009; Timmermans et al. 2007).

II. Calculations of Leaf Energy Balance: Basic Processes in the Steady State

A. Energy Balance Equation in the Steady State

1. Chief Components of Leaf Energy Balance

A useful place to begin is the calculation of the steady state, under constant radiation and atmospheric conditions and leaf orientation. I may write the energy-balance equation on a per-area basis (W m^{-2}) as the sum of radiative inputs minus outputs and of transfers of latent and sensible heat to the air:

$$0 = Q_{SW}^{+} + Q_{TIR}^{+} - Q_{TIR}^{-} - Q_{E}^{-} - Q_c - Q_s \tag{2.1}$$

Here, Q_{SW}^{+} is the energy flux density in leaf-absorbed shortwave radiation, arriving directly from the sun or scattered from other leaves, soil, etc.; Q_{TIR}^{+} is the energy flux density in absorbed thermal infrared radiation, which is contributed almost exclusively by atmospheric or "sky" radiation by water molecules combined with thermal emissions from leaves, soil, etc. – direct flux from the sun is negligible; Q_{TIR}- is the energy flux density in the TIR emitted by the leaves, acting nearly as classic blackbodies; Q_E-$= \lambda E$ is the flux density of latent heat, formulated as the flux density of water vapor from the leaf, E, multiplied by the latent heat of evaporation, λ; Q_c is the convective loss of heat to the air through the leaf boundary layer, and this may be positive or negative; and Q_S is the storage term, composed of thermal storage during transient heating (or, with a negative sign, cooling) plus chemical energy storage in photosynthesis (less respiration). Figure 2.1 presents a simple geometric sketch of the fluxes.

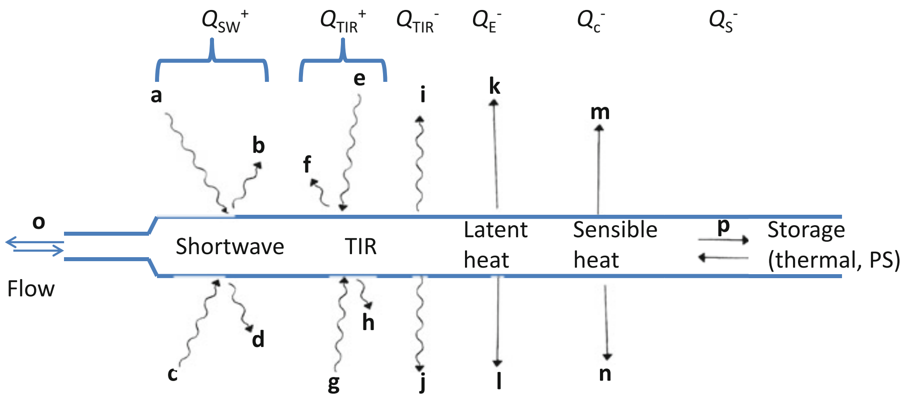

Fig. 2.1. Elements of energy balance of a flat-bladed leaf (not a needle or cladode), viewed edge-on. By convention, the top is the adaxial surface, though wind may invert a leaf. All the elements occur at each unit of surface area. Elements of net shortwave energy gain $\left(Q_{SW}^+\right)$: (*a*) shortwave radiation incident on nominal top or adaxial surface (UV, PAR, NIR); the illumination geometry must be known to compute this; it may include radiation reflected from other vegetative or soil surfaces (the leaf can twist in the wind to face the soil in part); (*b*) reflected shortwave radiation incident on the adaxial surface, computed from the sum of reflectivities in each band multiplied by the flux density in the band, plus transmitted shortwave radiation incident from abaxial surface; (*c*) shortwave radiation incident on the nominal bottom or abaxial surface; generally this is only radiation reflected from other surfaces; (*d*) reflected shortwave radiation from abaxial surface, plus transmitted shortwave radiation incident from the adaxial surface. Elements of net gain of thermal infrared (TIR) energy $\left(Q_{TIR}^+\right)$: (*e*) TIR incident on adaxial surface; a combination of sky emission and emission from terrestrial surfaces, weighted by associated fractional hemispherical views; (*f*) TIR radiation reflected from adaxial surface; typically only about 4 % of incident flux density; note that transmission of TIR radiation is negligible; (*g*), (*h*) corresponding fluxes from the abaxial surface. Elements of TIR loss $\left(Q_{TIR}^+\right)$ (*i*), (*j*) emission of TIR radiation by the adaxial and abxial surfaces, respectively, at the blackbody rate multiplied by the thermal emissivity; magnitudes of (*i*) and (*j*) are essentially equal because thermal gradients in leaves tend to be very small except on thick cladodes. Elements of sensible heat loss $\left(Q_E\text{-}\right)$: (*k*) loss from adaxial surface; (*l*) loss from abaxial surface, which may differ in magnitude from adaxial rate because the boundary-layer conductances differ between sides. Elements of latent heat loss $\left(Q_c\text{-}\right)$: (*m*) loss from adaxial surface; (*n*) loss from abaxial surface; again, magnitudes generally differ because of differences in boundary-layer conductances. Transport loss (not cited in text): (*o*) transport in xylem flow; typically very small; conduction along petiole is even smaller. Storage $\left(Q_s\text{-}\right)$: (*p*) thermal as heat gain, photosynthetic as chemical enthalpy gain

2. Role of Energy Flows in Transient Heating, Photosynthesis, and Respiration

The last term in the energy balance considered is energy storage, which is given with a negative sign because it subtracts from the energy at the leaf surface. Thermal storage occurs during transients. A sudden sunfleck heats the leaf mass, or a sudden shading cools the leaf mass. Thermal transients are discussed in Sect. IV.B. Photosynthetic carbon fixation (and nitrate reduction) represents chemical energy storage. This is typically small and often neglected in energy balance calculations. Consider the highest rates of photosynthesis observed, approximately 40 μmol CO_2 m^{-2} s^{-1}, which are about twice the highest rates of most crops and about 4 to 8 times the rates of common non-crop trees. The rate expressed as moles of glucose production is 1/6 that of CO_2 fixation, or about 6.7 μmol glu m^{-2} s^{-1}. The heat (enthalpy) of formation of glucose under standard conditions is about 2805 kJ mol^{-1}, to be moderately adjusted for the nonstandard conditions in the leaf (e.g., the partial pressures of CO_2 and O_2 are not 1 atm). Then, the rate of enthalpy storage is the rate of glucose formation, multiplied by the enthalpy stored per mole of glucose. The rate is then approximately 6.7×10^{-6} mol glu m^{-2} s^{-1} *

2.8×10^6 J mol^{-1} glu, or 17 W m^{-2}. This magnitude is to be contrasted with other energy flux densities, which in photosynthetic conditions are each typically several hundred watts per square meter. We may make similar arguments about the leaf respiration rate, which is typically a small fraction of the photosynthetic rate, often 8–10 % at most temperatures after leaves acclimate (Atkin et al. 2005; Wythers et al. 2005), with the bulk of respiration occurring in heterotrophic tissues of the plant or in soil organisms.

B. Defining the Individual Terms of the Energy Balance Equation

To use the original steady-state equation, we must resolve the individual terms, using driving variables such as solar radiation, leaf (essentially fixed) parameters such as shortwave absorptivities, boundary conditions such as atmospheric conditions, and temperature as a state variable. We can use the formula for the average T of a whole leaf or solve the equation segment-wise using the finite element method (Chelle 2005).

1. Shortwave Energy Input

Shortwave energy absorption is given as:

$$Q_{SW}^{+} = a_{PAR}E_{PAR} + a_{NIR}E_{NIR} \tag{2.2}$$

Here, the a's are absorptivities in the two wavebands (and we can consider resolving wavebands more finely) and the E's are energy flux densities in those wavebands, projected onto the leaf lamina normally. The absorptivities need to be measured, as they depend upon nutritional state (the difference between pale and dark leaves in a_{PAR} may be between 0.7 and 0.85 or higher), leaf hairiness and waxiness, and, to some extent, the angle of illumination. The lower side of the leaf typically has a lower PAR absorptivity. Absorptivity in the NIR is low, near 0.35, as indicated in numerous studies. More generally, absorption for radiation at any wavelength varies with the angle of incidence on the leaf. For diffuse radiation such as skylight that comes from many directions, a more comprehensive treatment is needed both in theory and in field measurement for accurate estimation of the absorbed fraction of radiation. One uses the concept of the bidirectional reflectance distribution function (BRDF; Schaepman-Strub et al. 2006; Chelle 2006; Chap. 11, Disney 2016). The BRDF describes the partitioning of radiation incident from one direction into reflected (and transmitted) radiation in all directions. Integration of the BRDF over all outgoing directions yields a fraction less than unity. This deficit is the absorbed fraction. This level of detail is not often demanded in simple calculations.

The values of E_{PAR} and E_{NIR} are composed of the direct solar energy flux densities and the scattered energy flux densities. Considerable complexity attends the calculation of the scattered radiation, as will be discussed in the section on leaves in canopies, but some useful simplifications are available. In some modeling efforts, the values of the solar energy fluxes will be given directly in energy units, as W m^{-2}. In other efforts, we may have available the quantum flux densities, in mol m^{-2} for the PAR, with the conversion that 1 mol of photons has roughly 220 kJ of energy. However, for precise conversion, one needs the spectrum of solar energy (Ross and Sulev 2000). It is unusual to have NIR energy flux density quoted in moles, and often it is not given; one must use the relation that the PAR and NIR energy flux densities in sunlight are nearly identical, with some finer approximations being available, particularly to correct for shifts caused by cloudiness, aerosols, etc. (Escobedo et al. 2009).

2. Thermal Infrared Input

Continuing, we may formulate the TIR input in terms of the energy flux density in the TIR band as

$$Q_{TIR}^{+} = \varepsilon E_{TIR} \tag{2.3}$$

Here, ε is the thermal absorptivity of the leaf, which equals its emissivity, by the physical principle of microscopic reversibility. The absorptivity is commonly very closely to 0.96, because it is dominated by the water content. Very waxy leaves may have modestly lower values. The incident TIR energy flux density, E_{TIR}, has, as noted, contributions from the sky and from terrestrial sources. Sky TIR, as we may call it, can be measured directly, with multiband radiometers. However, these are expensive and not used in most situations calling for modeling of leaf performance. Consequently, we usually need to use approximate equations that estimate E_{TIR} from ground-level weather variables, the air temperature and humidity. The TIR flux is continuously absorbed and emitted at all levels of the atmosphere. Accurate prediction requires a radiative transport model, and a knowledge of the distribution of the content of water (the by-far dominant TIR-active molecule) at all levels. For a standard atmospheric profile of temperature and water vapor content (not always the case!), the TIR emission of water molecules at all levels is prescribed, as is the transport of this TIR radiation with transmission, absorption, and reemission occurring at all levels. The transport equation can be solved, as it often is for satellite meteorology (Zhang et al. 2004) but more commonly a plant modeler will use an empirical relation, such as that of Brutsaert (1984):

$$E_{TIR} = \varepsilon_{sky,eff} \sigma T^4_{abs,sky} \qquad (2.4)$$

with σ as the Stefan-Boltzmann constant, $T_{abs,sky}$ (K) as the temperature of the air at screen height, and the effective emissivity of the sky as

$$\varepsilon_{sky,eff} = 1.72 \left(\frac{e_{air}}{T_{air,obs}} \right)^{0.143} \qquad (2.5)$$

where e_{air} (kPa) is the partial pressure of water vapor in the air at screen height. For air masses of low relative humidity, the effective sky temperature (representing the sky as a black body at this effective temperature),

$$T_{eff,sky} = \left(\frac{E_{TIR}}{\sigma} \right)^{\frac{1}{4}} \qquad (2.6)$$

can be many tens of degrees below air temperature, and the "deficit" in E_{TIR} relative to the value it would take at an effective emissivity of unity can exceed 150 W m^{-2}. The coldness of the sky in such conditions must be taken into account in accurate models of leaf energy balance. Note that clouds have high emissivities, near 1.00 (Hartmann 1994; Houghton 1977) and emit effectively at the temperature of their bases, which is T at screen height minus the lapse, which is likely to be simply the dry adiabatic lapse rate (ca. 10 K km^{-1}) multiplied by the cloud base height above ground level. For partly cloudy skies one must use both the clear sky and cloud values of E_{TIR} with weighting by fraction of sky coverage.

The contribution of terrestrial radiation sources to the TIR flux is complicated in plant canopies, as it is for shortwave radiation. The emissivity (equal to TIR absorptivity) of leaves is high, approximately 0.96, and most soils are similarly high, about 0.95, although low-iron sands may have emissivities of 0.90. The reflectivity $1 - \varepsilon$, is then low. There is very little reflected TIR inside canopies. As a result, one may estimate TIR fluxes from surrounding leaves, branches, soil, etc. as being their black body radiant flux densities at their body or kinetic temperatures. One then weights the contribution from all these surfaces in the proportion of solid angle each source subtends at the leaf in question. In a simple case, a layered canopy, one may with decent accuracy weight the flux density from each layer by the penetration probability of hemispherically uniform radiation from each layer to the layer of the leaf under consideration.

3. Thermal Infra-Red Losses

The TIR energy loss from the leaf surface, Q_{TIR}-, is rather simply formulated as

$$Q_{TIR}^{-} = 2\varepsilon\sigma T_{abs,leaf}^{4} \tag{2.7}$$

where T_{leaf} (K) is the leaf temperature. The factor of two originates from the leaf having two sides that are effectively at the same temperature, at least in the case of thin leaves. Very thick leaves, and the thick phyllodes of succulent plants, merit a formulation that accounts for their geometry and the T gradients around their periphery.

4. Latent Heat Loss

The latent heat loss by transpiration, λE_{leaf}, is readily expressed for leaves in the common condition of not having surface water, snow, or ice. In this case, water loss occurs from the leaf interior (water vapor partial pressure e_i) through the stomata and the leaf boundary layer to ambient air outside the boundary layer (water vapor partial pressure e_a). Using modern molar units for conductances (Ball 1987), we may write

$$E_{leaf} = g_{bs}\frac{(e_i - e_a)}{P_a} \tag{2.8}$$

or, more accurately to account for mass flow as well as diffusion (Farquhar and Sharkey 1982),

$$E_{leaf} = g_{bs}\frac{e_i - e_a}{Pa - \frac{e_i + e_a}{2}} \tag{2.9}$$

where water vapor partial pressures and air pressure are in Pa and g_{bs} is the total conductance of stomata and the boundary-layer acting as series resistances:

$$\begin{aligned} g_{bs} &= 1/(1/g_s + 1/g_b) \\ &= g_s g_b/(g_s + g_b) \end{aligned} \tag{2.10}$$

Here, g_b and g_s are the conductances of the boundary layer and of stomata for water vapor (moderately different from their conductances for heat or for CO_2; Ball 1987).

The values of e_a and P_a are typically obtained from weather data. The value of e_i is commonly taken equal the saturated water vapor partial pressure at leaf T, $e_{sat}(T)$, and is thus, a function of leaf T only. There are many useful analytical approximations for $e_{sat}(T)$ such as that from Murray (1967), here giving the result in units of Pascals:

$$e_{sat}(T) = 610.8exp\left(\frac{17.269T}{237.2 + T}\right) \tag{2.11}$$

For internal consistency, I note that there is generally a small correction for leaf water potential (ψ_{leaf}). This corrections given as $e_{sat}(T)\exp(\psi_{leaf}\ V_w/(RT))$, with V_w as the molar volume of water ($18 \times 10^{-6}\,m^3\,mol^{-1}$). For moderately low water potential of -1 MPa, this factor is about 1 – 1.8/2500, which is essentially negligible.

In conditions of modest wind speed, the leaf boundary layer is commonly laminar, and we can use a formula for leaves of uncomplicated shape (e.g., Campbell and Norman 1998):

$$g_b = a\sqrt{u/d_{leaf}} \tag{2.12}$$

where $a \approx 0.147$ mol m^{-2} s$^{-1/2}$ for a single side of a leaf and u (m s^{-1}) is wind speed at the leaf location, and d_{leaf} is a characteristic leaf dimension, transverse to the wind direction. For highly indented or irregular leaves the reader is referred to Gurevitch and Schuepp (1990). For leaves having stomata on both leaf sides, and with unequal distribution of stomatal conductance (g_s) for leaf lower and upper side (LI-COR Biosciences 2004) (Parkinson 1985):

$$g_b = \frac{(1+K)^2}{K^2+1}g_{b,1} \tag{2.13}$$

with K being the ratio of g_s on the two sides of the leaf, and $g_{b,1}$ being the one-sided boundary-layer conductance. I note that this equation refers to calculation of water vapor and CO_2 transfer conductance from ambient air to leaf intercellular air space (Eqs. 2.8 and 2.9) not for calculation of transfer conductance for heat exchange.

For high wind speeds, the boundary layer can become mixed laminar-turbulent, and the leaf dimensions can change from leaf rolling (Alben et al. 2002; Jarvis and McNaughton 1986 – see p. 42). Leaf fluttering can alter g_b and can occur at low wind speeds, as in the iconic quaking aspen, *Populus tremuloides* (Roden and Pearcy 1993). At very low wind speeds, convection undergoes a transition from forced convection by external wind toward free convection driven by thermal gradients in the air. At the free-convection limit, we have

$$g_b = \alpha \left(\frac{T_{leaf} - T_{air}}{d} \right)^{\frac{1}{4}} \tag{2.14}$$

with $\alpha = 0.05$ mol $m^{-\frac{7}{4}}$ $s^{-1}K^{-\frac{1}{4}}$ There are formulas for intermediate cases (Kreith 1965; Schuepp 1993). While anything approaching free convection is rare under weather conditions in which photosynthesis occurs at a significant rate, the time intervals in which free convection occurs can be important for photosynthesis at other times of day. Ball et al. (2002) give a classic example from snow gum (*Eucalyptus pauciflora*) seedlings in an Australian forest clearing in wintertime. Pre-dawn and immediately post-dawn, u is near zero, giving a very low value of g_b and thus of convective heat transfer rate, Q_c-. Radiative energy balance becomes critical; leaf T drops about 2–4 °C below air T. Leaves freeze, but the damage to photosynthetic capacity arises almost exclusively from photoinhibition, in turn caused by very low T and high solar irradiance on leaves.

To continue, we must also know the value of stomatal conductance, g_s, in order to compute latent heat flux density from the leaf. A simple solution of the energy balance equation is possible if this is a known, fixed value.

5. Convective Heat Exchange

Finally, I the basic formula for the convective heat-loss rate is:

$$Q_C^- = g_{b,h} C_{P,air} \left(T_{leaf} - T_{air} \right) \tag{2.15}$$

where $g_{b,h}$ is the boundary-layer conductance for heat (about 0.92 that for water vapor; Campbell and Norman 1998) in usual molar units and $C_{P,m}$ is the molar heat capacity for air. Of course, the flux density can be negative under advective conditions when the air is hotter than the leaves.

6. Solving the Leaf Energy Balance Equation

Once we have all the terms in the energy-balance equation, we have a form in which all quantities are fixed other than leaf T, and one may apply any of the iterative schemes to find the steady-state temperature. No precise analytic solution is possible because the equation is transcendental in T: the TIR emission from the leaf, Q_{TIR}-, is quartic in T, the convective loss, Q_c, is linear in T, and the latent heat loss is approximately exponential in T. An iterative solution is almost always affordable (Box 2.2). In addition, various approximate solutions have been proposed that in general provide a good approximation of leaf temperature (Paw 1987; Greek et al. 1989), and under certain assumptions leaf energy balance can be calculated using a quadratic analytical solution (Baldocchi 1994).

Box 2.2 Iterative Solution of the Leaf Energy Balance Equation

One can guess the value of T and then use the Newton-Raphson method of root-finding. Expressing the energy-balance equation as $f(T) = 0$, we assume that, at any T, $f(T)$ is nearly linear in T in some small neighborhood, or $f(T + dT) \approx f(T) + f'(T)\, dT$. If $f(T)$ at the estimated T is nonzero, we can posit that there is a dT that

(continued)

Box 2.2 (continued)

makes $f(T + dT) = 0$, or $dT = -f(T)/f'(T)$. This will give an improved value, which we may then improve in the next iteration until $f(T)$ is sufficiently small, say 1 W m^{-2} or less. The values of $f(T)$ and $f'(T)$ can easily be computed numerically using the very accurate analytic formulas for the partial pressure of water vapor, which generates a corresponding analytic formula for the derivative with respect to T. For example, if we use Eq. (2.12) above, the derivative of $e_{sat}(T)$ is e_{sat} itself, multiplied by the factor $(17.269*237.2)/(237.2 + T)^2$. At 25°, this factor is 0.060; that is, saturated water vapor pressure rises 6 % per degree Celsius. In the iterations for T using the Newton-Raphson method, it may be necessary to hobble the increments, dT, to perhaps 3–5 °C to avoid overshoots and oscillations.

An inherently stable alternative method of solving the transcendental equation for T is a binary search (Burden and Faires 1985), one of several such numerical root-finding methods (McCalla 1967). For a monotonic function such as energy balance with only one real root, the process is straightforward. A binary search for the root of an equation $f(T) = 0$ begins with the evaluation of $f(T)$ at two endpoints that are estimated to contain a root. Consider a notional case in which at the lower limit, T_0, $f(T)$ is positive, and at the upper limit, T_1, it is negative. One then knows that the root lies between these points. One then evaluates $f(T)$ at the midpoint, which we may call T_2. Suppose that $f(T_2)$ shows up as a negative value, indicating that the root lies between T_0 and T_2. One then makes T_2 the new upper limit in the search. The search continues, with evaluation at T_3, which, with $f(T_3) < 0$, clearly becomes the new lower limit, and so on. Binary searches are rapid, halving the uncertainty each iteration or by $1/2^n$ in n iterations. An initial search interval of 10 °C drops to <0.1 °C in 8 iterations. The modest disadvantage of a binary search is that it requires significantly more lines of code that a simple Newton-Raphson iteration, especially when one includes adaptive expansion of the search limits if the initial endpoints do not encompass a root (e.g., $f(T)$ is positive at both points, or negative at both points).

C. Leaves in Artificial Environments: Growth Chambers, Greenhouses, and Warming Experiments

Similarly to sunlight, the terms in the energy balance equations are the same for leaves in any other situation, and they may be measured by the same or equivalent means, e.g., PAR meters, anemometers, etc. There is one change that is often overlooked when artificial illumination is used, the change in TIR input to the leaves. The sun emits negligible TIR in comparison to its shortwave (SW) radiation in the PAR and NIR. In contrast, growth lamps emit even more TIR than SW radiation – about 3-fold more for fluorescent lamps, and 20-fold more for incandescent lamps, which no modern system uses, except when perhaps supplementing gas-discharge or fluorescent lamps by far-red light. One must account for the increased TIR in modeling plant growth in a growth chamber or artificially illuminated greenhouse, unless the TIR has been filtered out. This filtering can be achieved with a water-filled plenum between the lamps and the plants (Gutschick et al. 1988). In addition, as the energy decreases with the square of distance from the light sources, energy gradients within vegetation are much greater in artificial growth conditions than in outside where the energy source distance effect is negligible, at least for PAR and NIR (Chelle et al. 2007; Delepoulle et al. 2009; Niinemets and Keenan 2012). Furthermore, even outdoors, modelling plant energy balance in artificial environments such as cities is complicated due to shading effects and different optical and heat capacitance characteristics of buildings.

The copious emission of TIR by lamps is used to effect in outdoor warming experiments (e.g., Kimball 2005). The effect, however, is not equivalent to the warming of air under climate change. Put most simply, the topmost leaves warm the most and lower leaves less so, because the interception of TIR by leaves above a location depletes the TIR flux density and the energy density is also reduced by distance from TIR source (depending in the geometry of used TIR source). To put it another way, the flux of TIR is vectorial, not equivalent to a uniform change in scalar air temperature. The degree of unrealism is not readily assessed. While upper leaves contribute most to photosynthesis, respiration, and transpiration, there is an extra gradient in leaf temperature through the depth of canopy, over and above the one that develops naturally from differential interception of SW radiation and other effects. This may affect development and fruiting.

D. Detection of Leaf Temperature and of Energy-Balance Components

Although difficult, validation of modeled leaf energy balance and leaf temperature is a necessary pursuit. Models predict the kinetic temperatures of leaves. These temperatures can be measured by contact methods such as thermocouples. Sampling many leaves, at various canopy locations and leaf angular orientations, can easily become impractical. I may relate an amusing anecdote from Marilyn Ball of the Australian National University. Decades ago, the renowned modeler Ian Cowan decided to do a field experiment, in which he added a very large number of sensors, including thermocouples, to a plant. The results were confusing, until it was realized that Cowan had accidentally kicked the plant at its base and severed its stem; only the sensor wires alone were holding the plant up. Even in experiments unconfounded by damage, the presence of a large number of sensors and their stiff or weighty wiring can add artifacts to the results.

The common alternative to contact measurement is measuring the TIR emission by the leaves. The most affordable instruments, simple infrared "guns" or infrared thermocouples, do not image the area being viewed; rather, they average a finite solid angle. Their view into a canopy depends upon the orientation of the sensor, the canopy structure (esp. as row crops), and the position of the sun. Kimes et al. (1981) and many others (e.g., Lagouarde et al. 1995; Smith et al. 1997; Kustas et al. 2007) have analyzed this challenge, without a simple answer, because the question is not simple: does one want the average leaf *T* or that of a specific canopy stratum? Does one want the average leaf T weighted by area, or by transpiration rate, or by photosynthetic rate? A step toward resolving the problem is using imaging TIR cameras that provide a spatial distribution of leaf temperatures. However, they are quite costly, typically US$ 10 K or more. Some informative results have come forth, including use of thermal imagery to infer the spatial distribution of stomatal conductance (Fig. 2.2; Jones et al. 2002; Leinonen et al. 2006).

For large-scale sensing, such as from satellites, imaging of leaves is impossible. This results in significant problems and inaccuracies in the interpretation of surface (canopy) *T* for inference of stand transpiration rates, by methods that are discussed in Sect. VI. Many satellite sensors such as MODIS cover wide areas at semi-oblique angles. The spread in view angles incurs the problem of radiative *T* varying with view angle, noted at the beginning of this paragraph. Satellite remote sensing faces an additional problem, that of distortion of the TIR signal by absorption and emission of TIR in the atmosphere between the satellite and the plant. A great deal of work has gone into deriving accurate models that extract the TIR signal at the surface. The claim for MODIS TIR data is that the inferred surface temperatures are accurate within a standard deviation on the order of 1 °C (Wan et al. 2004).

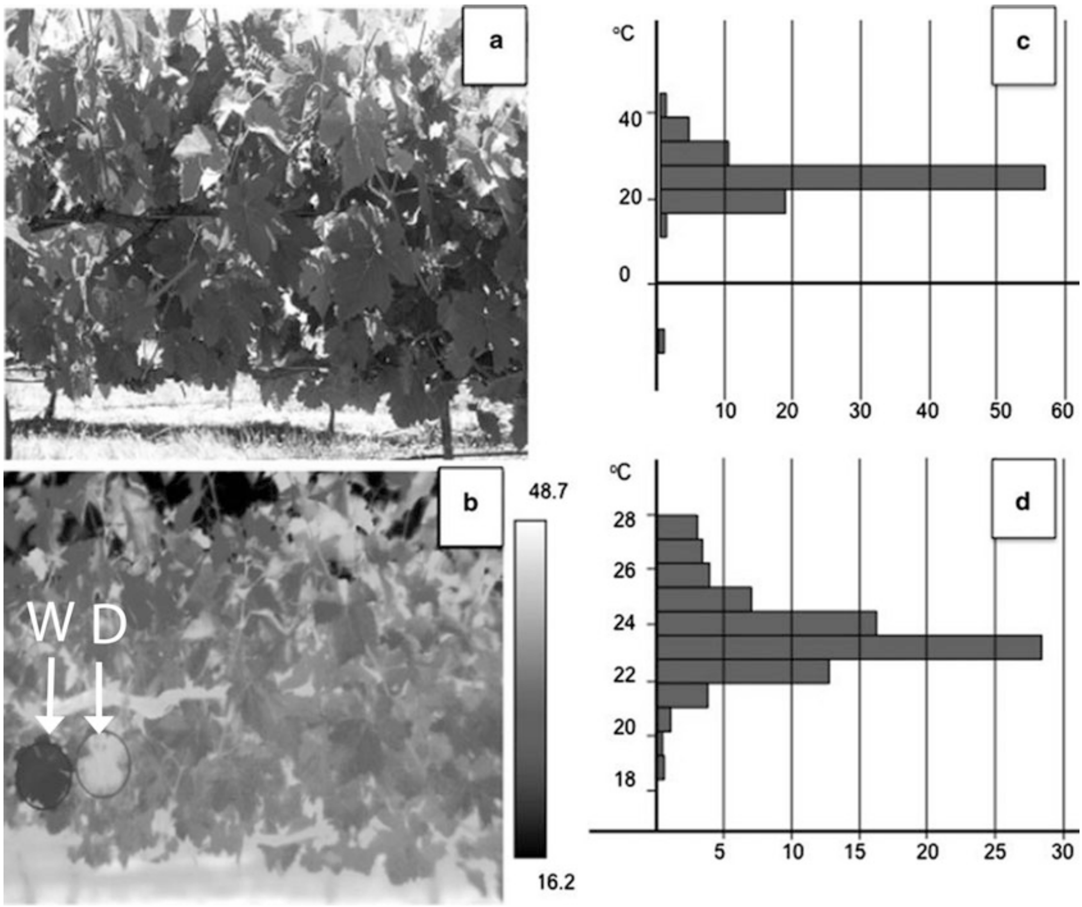

Fig. 2.2. Optical (**a**) and thermal imagery (**b**) of a grapevine canopy in midday, showing a wide range of leaf temperatures arising primarily from varied interception of solar shortwave radiation at varied leaf angular orientations. *Arrows* point to reference leaves that are wet and cool (W) and dry and hot (D). Histograms of temperature derived from thermal imagery are presented for the complete scene (**c**) and for leaves only (**d**), i.e., excluding hot soil and "cold" sky. Minimally modified from Fig. 2.1 of Fuentes et al. (2005) – converted to grayscale, with addition of more obvious arrows for reference leaves in panel (**b**); lower end of temperature scale for panel (**b**) corrected to +16.2 °C from −16.2 °C; used with permission

E. Meeting the Challenges of Measurement and Theory

Using the concepts of energy balance is clearly fraught with a number of challenges. Some arise from limitations of data. One challenge that is rife, especially for studies over large areas or multispecies assemblages is, Can one measure enough parameters such as optical absorptivities, stomatal control parameters, or photosynthetic capacities to predict energy balance and the processes linked to it? One lead here is that there are often rather robust approximations suitable for initial studies. For example, in stomatal control modeled with the Ball-Berry formula (Ball et al. 1987), the slope parameter is close to 10 for most species that have the C_3 photosynthetic pathway (Gutschick and Simmoneau 2002).

Other challenges arise from conceptual complexity and attendant mathematical complexity. Conceptual complexity is not, however, conceptual uncertainty;

biophysical and physiological theory is well developed. Admittedly, one often needs to develop simplifications to reduce complexity. One may simplify the description of radiative transport within a plant canopy, perhaps using two-stream models of upward- and downward-propagating radiation (Liang and Strahler 1993; extensions by Gutschick and Wiegel 1984; Dai and Sun 2006). One must be aware that the approximation must be tested and that its accuracy is likely to vary with canopy structure, such as leaf angle distribution. Mathematical complexity succumbs to mathematical abilities, which might be effectively "contracted out" to collaborators or else dug out of the literature. Even the coupled nonlinear processes of energy balance, photosynthesis, stomatal control, and scalar transport in leaves became tractable long ago, as in the work of Collatz et al. (1991; see also Sect. III.C here). Computational complexity, that is, generating a computer program to handle the math and to run at an affordable rate, is often only weakly related to mathematical complexity. A very large number of equations that are inherently linear or well approximated by linearization can be handled readily by linear algebra, even with very many variables. On the other hand, problems that are simply formulated mathematically, such as the classic traveling salesman problem or the box-packing problem (engaging popular account by Graham 1978) have no algorithms short of trying every possible choice. Powerful approximation methods do exist for these, including simulated annealing (Kirkpatrick et al. 1983; Gershenfeld 1999) and genetic algorithms (Gershenfeld 1999). Raw computing power has ceased to be the limiting factor for most problems in the field of biology, certainly not being problematic for energy balance.

Experimental measurement and the design of experiments pose some persistent problems. Estimating transpiration from fields or landscapes (or its reduction, as a measure of stress) by remote sensing relies on measuring thermal radiation from the surfaces, primarily. Radiation moves as a vector, in straight lines, but actual kinetic temperature that conditions the transpiration rates of leaves is a scalar. Its spatial distribution is sampled with different weightings as the view angles of the radiation sensor change, as noted above. One gain on the problem is recognition that one must be clear about which spatially integrated temperature one wants. Is it weighted by canopy scalar transport capacity, for calculating sensible heat flux? Is it weighted by, primarily, stomatal conductance for calculating canopy transpiration? One might develop empirical relations between radiative temperature (perhaps over several view angles) and the fluxes one wishes to measure. One must be aware that these measures will be fairly specific to the canopy physical structure, for one. One might also add in models of photosynthesis and stomatal conductance to get a more general method. Good problems for future research await being addressed.

III. Physiological Feedbacks Affecting Leaf Energy Balance

In a free-running model of a plant canopy, which predicts all fluxes from plant parameters and driving variables, one must model the stomatal conductance of any given leaf from biochemical and physical processes, which depend upon leaf temperature. In effect, we must solve simultaneously the equations for energy balance, photosynthetic rate, stomatal conductance, and CO_2 transport, all but one (transport) being nonlinear.

A. Dependence of Stomatal Conductance on Environmental Drivers

Stomatal conductance to water vapor, g_s is tightly linked to very temperature-dependent photosynthetic rate itself, as expressed in various useful empirical formulas. I use here the seminal formula of Ball et al. (1987), which has been modified (see esp. Leuning 1995 and Dewar 2002), but often found as accurate as the modified versions (e.g., Gutschick and Simmoneau 2002; Chap. 3 Hikosaka et al. 2016a):

$$g_s = m_{BB}\frac{Ah_s}{C_s} + b_{BB} \tag{2.16}$$

Here, m and b are empirical constants, with surprisingly low variation among well-watered plants (Ball et al. 1987; Collatz et al. 1991; Gutschick 2007), A is the net photosynthetic rate, and h_s is the relative humidity and C_s the CO_2 mixing ratio, both at the leaf surface, beneath the boundary layer. The values of m_{BB} and b_{BB} are sensitive to water stress (Gutschick and Simmoneau 2002). The formula for h_s is simply e_s/e_i, with e_s defined as the saturated water vapor pressure at the leaf surface. We can solve for e_s considering that in the steady-state the leaf transpiration rate,

$$\begin{aligned} E &= g_b\frac{(e_s - e_a)}{P_a} = g_s\frac{(e_i - e_s)}{P_a} \\ \rightarrow h_s &= \frac{e_s}{e_i} = \frac{\left(\frac{e_a}{e_i} + \frac{g_s}{g_b}\right)}{\left(1 + \frac{g_s}{g_b}\right)} \end{aligned} \tag{2.17}$$

We need to determine A as a function of temperature in a way that is consistent with transport through the combined conductance of CO_2, g_{bs}', which uses the expressions relating conductances for CO_2 to conductances for water vapor,

$$g_b' = 0.72g_b, \quad g_s' = 0.62g_s \tag{2.18}$$

B. Biochemical Limitations of Photosynthesis

Photosynthesis has both light-limited regimes ($A = A_{LL}$) and light-saturated regimes ($A = A_{sat}$), with a good approximation for any light level being (Johnson and Thornley 1984; Farquhar et al. 1980)

$$\vartheta A^2 - (A_{LL} + A_{sat})A + A_{LL}A_{sat} = 0 \tag{2.19}$$

Here, A is the *gross* rate of CO_2 fixation, excluding respiratory losses, θ is a transition parameter; at $\theta = 1$, A shows a completely sharp transition between regimes; typical values seen in studies to date cluster around 0.8 (variation discussed by Jones et al. 2014). The net rate of CO_2 fixation is the gross rate debited for "dark" respiration, R_d. More or less complex models of dark respiration exist. A simple one is that it acclimates as a fairly constant fraction of net photosynthesis at the mean temperature of the photoperiod in the preceding week or two (T_{mean}; see Sect. II above; Wythers et al. 2005), varying with the diurnal temperature cycle as a simple exponential activation such as exp[0.07 $(T - T_{mean})$].

The biochemical expressions for A_{LL} and A_{sat} have been elegantly simplified in the work of Farquhar et al. (1980, with later elaborations). For C_3 plants, we have commonly

$$A_{sat} = V_{c,\max}\frac{(C_i - \Gamma^*)}{(C_i - K_{CO})} \tag{2.20}$$

where $V_{c,\max}$ is the maximal ribulose 1,5-bisphosphate carboxylation capacity, Γ^* is a hypothetical compensation partial pressure without dark respiration, but accounting for photochemical carbon oxidation or "photorespiration", and K_{CO} is an effective Michaelis constant for enzymatic binding of CO_2 to the rate-limiting Rubisco enzyme, and C_i is the CO_2 partial pressure inside the leaf; accuracy is gained by using C_c, the partial pressure at the carboxylating enzyme, Rubisco, in the chloroplasts (Niinemets et al. 2009). C_c is lower than C_i due to a significant CO_2 diffusion resistance in the gas, liquid and lipid phases from substomatal cavities to chloroplasts. $V_{c,\max}$, Γ^* and K_{CO} are functions of temperature, and $\Gamma^*$and K_{CO} are functions of the partial pressure of oxygen. This form applies when CO_2 fixation by Rubisco enzyme is the limiting factor. In some conditions, electron transport or triose-phosphate transport may be limiting (Farquhar et al. 1980; Wullschleger 1993).

Similarly, we have the light-limited rate as an "initial quantum yield," ϕ, multiplied by the photosynthetic quantum flux density, I_L, which may be expressed either as incident or absorbed light:

$$A_{LL} = \phi I_L = \phi_0 \frac{(C_i - \Gamma)}{(C_i + 2\Gamma)} \tag{2.21}$$

Here, ϕ_0 is the quantum yield at saturating CO_2 levels. As an example, we may consider the completely light-saturated case. We equate the biochemical and transport formulations for net photosynthesis, A, to obtain

$$A = V_{c,\max} \frac{(C_i - \Gamma^*)}{(C_i - K_{CO})} - R_d = g'_{bs} \frac{(C_a + C_i)}{Pa} \tag{2.22}$$

Here, C_a is the partial pressure of CO_2 in ambient air. We can multiply both sides by $(C_i + K_{CO})$ to obtain a quadratic equation in C_i, which can be solved explicitly. One can then insert the value of C_i into either equation to obtain the value of A. Note that a more accurate form for the transport relation requires consideration of mass flow (Farquhar and Sharkey 1982),

$$A = \frac{g'_{bs}(C_a - C_i)}{P_a} - \frac{C_i + C_a}{2P_a} E_{leaf} \tag{2.23}$$

which creates a modest complication in the solution. The correction to A due to mass flow is on the order of 5 % for a mesophytic C_3 plant with relatively high transpiration rate.

In the more general case, one can use the Johnson-Thornley expression for A, expressing both A_{LL} and A_{sat} in terms of C_i (→ just algebra; needs no reference). One gets a quartic equation in C_i, which can be solved by a binary or golden-ratio search (http://en.wikipedia.org/wiki/Bisection_method).

C. Solving a Combined Stomata-Photosynthesis Model

With these methods to estimate A, we are ready to get a consistent solution for photosynthetic rate, stomatal conductance, energy balance, and CO_2 transport. An analytic solution is available that however requires definition of a few additional constraints (Baldocchi 1994). In my own work, I find an effective algorithm to be:

- Set up a range of g_s over which to do a binary search
- At any given estimate of g_s, leaf energy balance is set, and so is T
- The value of T sets the values of the biochemical parameters $V_{c,\max}$, Γ^*, and K_{CO}
- The value of C_i can be solved, as just noted, and thus we can obtain the value of A. We also obtain the value of $C_s = C_a\text{-}AP_a/g'_b$
- The function whose root is to be sought uses the Ball-Berry equation, or similar equation of one's choice. One composes $f(g_s) = g_s - (m_{BB}Ah_s/C_s + b_{BB})$, and seeks for the root $f(g_s) = 0$.

The binary search is relatively rapid computationally and stable. One needs reasonable estimates of the search interval in g_s, and programming that allows expansion of the range if no root is evident in the initial range. This whole method has been programmed and is available from the author as a standalone program in Fortran 90 source code or as a Windows executable. I have also used inverse modeling in a larger model of climate change impacts in which the above model is at the core. The exercise may be of interest to modelers (Gutschick 2007). The inverse model inferred plant physiological parameters from final performance measures, such as photosynthesis, transpiration, and nitrogen-use efficiency. I then projected (variable) changes in the physiology to do forward modeling of new values of final plant performance measures. A whole-plant model of these coupled processes, including water transport and water potential, has been constructed (Tuzet et al. 2003). Fig. 2.4 presents a flowchart of the calculations presented to this point. Gutschick and Sheng (2013) present more

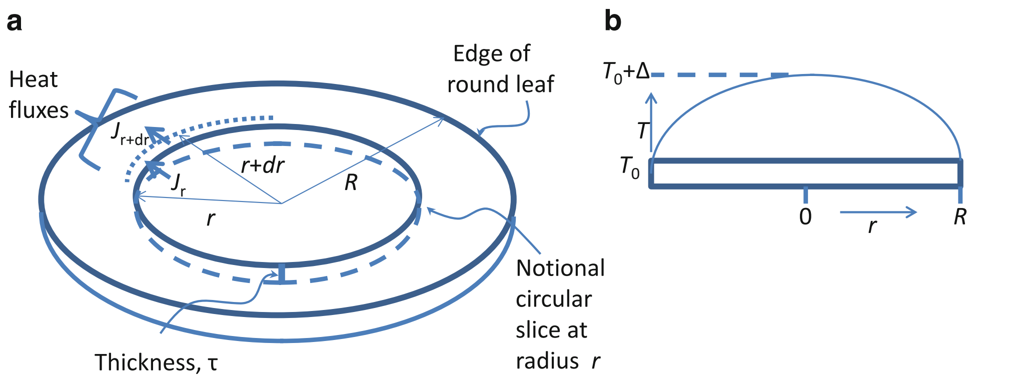

Fig 2.3. Geometry of radial heat flux in a round leaf. (**a**) Slant view of leaf. Azimuthal symmetry of temperature and heat flux is assumed. Flux J_r crosses the area given by the perimeter at radius r multiplied by depth (thickness) τ. Flux J_{r+dr} crosses the area at radius $r + dr$. (**b**) Notional temperature gradient treated in the text is a parabolic function of radius r, peaking at the center at temperature $T = T_0 + \Delta$ in the center and falling to $T = T_0$ at the edge

complete computational details from their study using a model that also treats leaves within the environment set by a complete canopy (see Sect. IV, below).

The strong coupling of the various processes is evident in simulations using varied values of environmental driving variables such as air temperature and of plant parameters such as photosynthetic capacity, $V_{c,\max}$. Evolutionary selection pressure is also implied in the form of the stomatal control program. The Ball-Berry form tends to preserve water-use efficiency by coupling changes in the various processes (Gutschick 2007).

Schemes for predicting the coupled behavior of energy balance, photosynthesis, and transport, such as the one just described, certainly are complex. One might hope for an equation that expresses any flux such as A directly in terms of the driving variables (PAR and NIR flux densities; wind speed; air temperature, relative humidity, and CO_2 partial pressure) and plant parameters (optical properties, photosynthetic parameters, stomatal control parameters, and leaf dimension). This equation would have to be derived by a high-dimensional fitting of data, such as by nonlinear least squares. Although such an equation could be potentially derived, it seems wholly impractical.

D. Advanced Problems

There are several extensions of the technique outlined in Sect. III.C. Foremost, the enzyme-kinetic form for C_4 plants differs from that for C_3 plants used here in the example. The C_4 formulas have been developed, including variants that account for CO_2 leakage out of the bundle-sheath cells (Jenkins 1997; von Caemmerer and Furbank 2003). Collatz et al. (1991) used these in providing a solution of the combined equations of photosynthesis, stomatal conductance (with the Ball-Berry model), energy balance, and CO_2 transport. Note also that the value of C_i is affected by mass transport of water vapor that opposes the inflow of CO_2; corrected expressions are given by Farquhar and Sharkey (1982).

Greater complications arise from the presence of liquid water, ice, or snow on the leaf surface. The least complicated case may be that of dewfall on a leaf with essentially closed stomata. In this case, water vapor flows from air to the leaf surface, releasing the heat of condensation, of magnitude λ times the rate of water condensation on surface. Dewfall will not occur during times when leaves have even modest sunlight interception, but the load of dew must be evaporated during the latter times. Energy balance is clearly affected by this extra source of water vapor flux away from the leaf. Photosynthesis is also affected by water droplets or films blocking stomata on the upper leaf surface (Hanba et al. 2004). The formulation of dewfall rate as a function of atmospheric conditions, TIR radiative balance, and leaf orientation is beyond the scope of this chapter. Similarly, I leave the discussion of the melting, dripping, and sublimation of ice and snow from leaves to more specialized publications (e.g., Gelfan et al. 2004; Ni-Meister and Gao 2011). This is not to imply that snow and ice dynamics on leaves are relatively unimportant. The vast regions of boreal forest, tundra, and other ice-prone areas are important in climate and the carbon and water cycles on spatial scales from region to globe.

IV. Transients in Energy Balance and in Processes Dependent on Temperature

A. Independence of Different Leaf Regions

We may omit conduction of heat through the petiole or even between different regions of the leaf lamina. The argument is based on a consideration of numerical magnitudes. Consider a leaf of the type that may develop a large gradient in temperature laterally, such as a wide leaf in strong sunlight at low airflow (low boundary-layer conductance, g_b). A sunflower leaf is a good example (Guilioni et al. 2000). For simplicity, consider the T gradient to be (admittedly crudely) radial on a circular leaf, which has a thickness τ (Fig. 2.3). An annulus lying between r and $r + dr$ has a cross sectional area across the thickness of $A = 2\pi r\tau$. The net flow of heat, J, between heat moving in at radius r and heat moving out at radius $r + dr$ is

$$\begin{aligned} J &= A(r)k_{th}\frac{\partial T}{\partial r}\Big|_r \\ &\quad + A(r+dr)k_{th}\frac{\partial T}{\partial r}\Big|_{r+dr} \\ &\rightarrow Ak_{th}\frac{\partial^2 T}{\partial r^2} \end{aligned} \tag{2.24}$$

This is the heat input into the annulus (a ring) having a surface area $2\pi r\, dr$, such that the heat flux density, Q, per unit area of the annulus is the expression above divided by this area, or, using $A = 2\pi r\tau$ again,

$$Q = \tau k_{th}\frac{\partial^2 T}{\partial r^2} \tag{2.25}$$

For a leaf thickness of 200 µm with a quadratic gradient in T covering, say, 8 °C over a final radius R, the second partial derivative is $-16\ K/R^2$. Using the thermal conductivity as that of water, about 0.6 W m^{-1} K^{-1}, we estimate Q as 0.53 W m^{-2}. This is wholly negligible compared to all other terms in the energy balance. A conclusion we may draw is that energy balance may be considered independently for various segments of a leaf that have developed different boundary layer thicknesses (from differences in distance from the leaf leading edge in the wind) or are displayed at different angles to sunlight. The differences can be important for the temperature-dependent processes of leaf or floral initiation (ibid.).

B. Dynamics in Leaf Temperature After Changes in Energy Balance Components

1. Time-Dependent Changes in Temperature After Modifications in Radiation Input

Leaves flutter in the wind, sunflecks come and go. Consequently, the terms in the energy-balance equation shift, as does leaf temperature and the T-dependent processes in the leaf such as photosynthesis. In many cases, it is appropriate to average the leaf performance among the varying conditions, weighting performance contributions by the

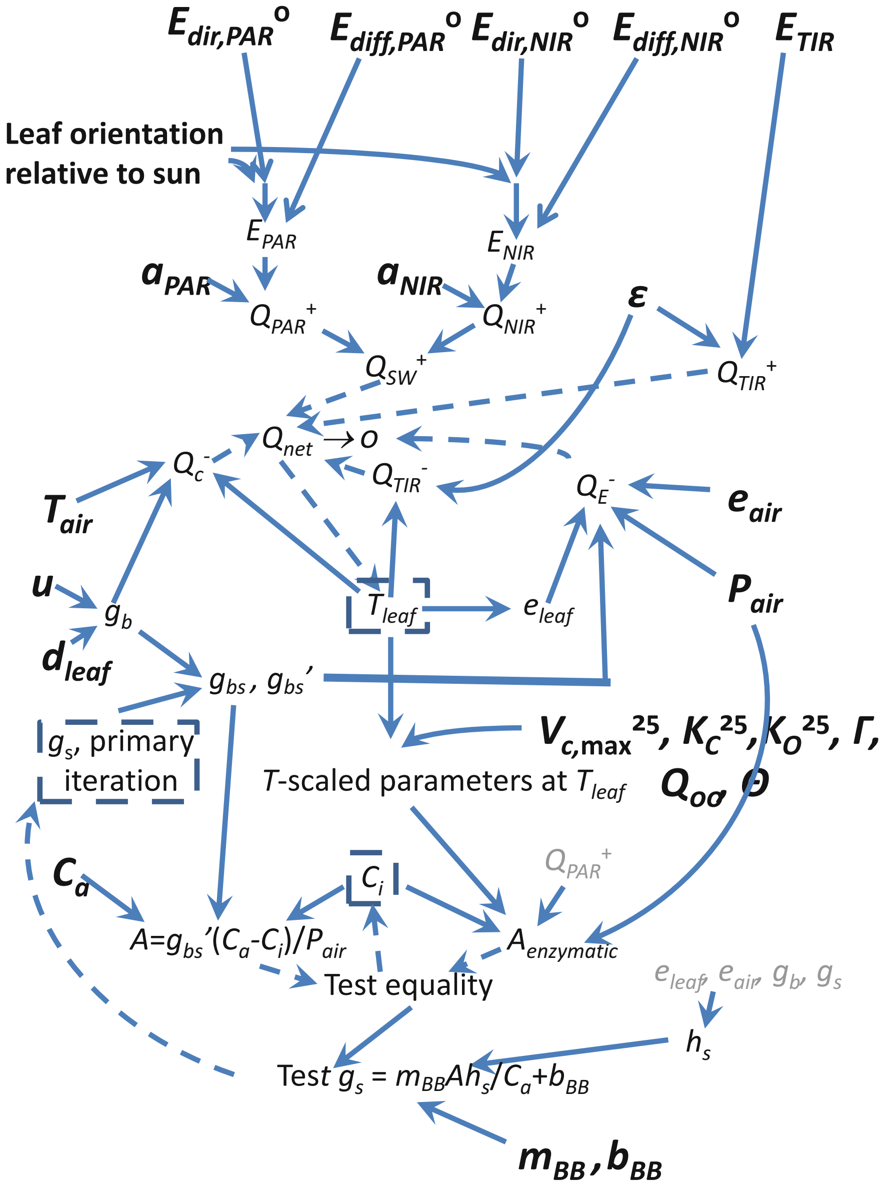

Fig. 2.4. Flowchart for fully mechanistic calculation of energy balance and accompanying fluxes, for an isolated leaf in fully specified environmental conditions. Entries in *large boldface* text are fixed environmental conditions in assumed steady state, as well as fixed physiological, optical, and structural properties of a leaf blade. All other quantities are results of calculations. Shaded quantities are repeated from other locations in the diagram rather than using long arrows from other locations that add complexity. Notation generally follows that in the text, with some added detail, such as expanded subscripts to distinguish contributions of direct and diffuse energy flux densities in the PAR and NIR wavebands (compare simpler notation in Eq. 2.2 in the text). *Solid arrows* indicate forward calculations using equations given in the text or related publications. *Dashed arrows* indicate feedback of results for iterative correction of quantities at the arrow heads with new input values. With all environmental conditions and parameters being set, the origin of iterations is setting the stomatal conductance, g_s, leading to estimation of evaporative heat loss, Q_E-. This allows, in turn, estimation of leaf temperature (T_{leaf} here, for clarity; denoted T_l in text). After leaf temperature estimates have converged, the photosynthetic rate is computed iteratively by adjusting leaf internal CO_2 partial pressure, C_i, so that the rate computed from transport through stomatal and boundary-layer resistances (A in equation on *right* near *bottom*) equals the rate computed from enzyme kinetics ($A_{enzymatic}$, as in Eqs. 2.20, 2.21, 2.22, and 2.23 in text). The value of g_s is then compared to the value required for consistency with the stomatal control model, here given as the Ball-Berry form (Ball et al. 1987; Eq. 2.16 in text). A difference greater than a chosen tolerance incurs iteration with a new value of g_s, chosen effectively with a binary search method

Table 2.1. Representative flux densities, W m^{-2}. Q_S- from photosynthesis, except (*th*) = thermal

Condition	Q^+_{SW}	Q^+_{TIR}	Q_{TIR}-	Q_E-	Q_c-	Q_S-
Crop, full sun; warm, dry	550	800	900	400	50	5–18
Crop, night; warm, dry	0	700	800	≈0	−100	−0.5 to −2
Needle leaf; lower sun, cool	200	650	700	100	50	0–2
Desert evergreen; low sun, winter	150	650	700	50	50	0–3
Crop, sunfleck; warm, dry	550	800	850 → 900	100 → 400	0 → 50	400 (*th*) → 0

fraction of time spent in each condition. There are, however, cases in which transient behavior is very important. Both measurements and models have been made on understory plants that see infrequent sunflecks of short duration (Chazdon and Pearcy 1991; Pearcy et al. 1997). The plant must accomplish its photosynthetic carbon gain in these sunflecks with rapid adjustments of stomatal conductance and of the activation state of Rubisco. The latter phenomena merit discussion in other venues and in other chapters in this book. Here, we may consider the transient behavior in leaf energy balance and temperature. The energy-balance equation modified for time-dependent behavior must account for the net rate of heat gain, *J*,

$$Q^+_{SW} + Q^+_{TIR} - Q^-_{TIR} - Q^-_E - Q_c = C_{P,a}(dT/dt) \tag{2.26}$$

Here, $C_{P,a}$ is the heat capacity of the leaf per unit area, which is simply the heat capacity per unit leaf fresh mass multiplied by the fresh mass per unit leaf area. If the leaf is 20 % dry matter, its heat capacity per mass is 0.8 times the heat capacity of water, about 4200 J kg^{-1} K^{-1}, plus 0.2 times the heat capacity of dry matter, 1000 J kg^{-1} K^{-1}. This yields a heat capacity per mass of 3560 J kg^{-1} K^{-1}. Per area, the heat capacity is the value per mass multiplied by the mass per area. In Table 2.1, to be explained shortly, one example is a thin leaf, 0.2 mm thick, with 0.2 kg of fresh mass per square meter. The heat capacity per area, $C_{P,a}$, is then 712 J kg^{-1} m^{-2}. Now consider a leaf in which the terms in Eq. 2.1 shift from an initial steady state. A very common case is a change in a direct energy input, as a change in shortwave energy input (change in sunlight amount). Let the change in Q^+_{SW} be by an amount δ. Let the original values of the energy terms be denoted with an additional subscript "0" (e.g., $Q^+_{SW,0}$) and their derivatives with respect to temperature be denoted by appropriately subscripted quantities b_i. For example, $(d/dT)Q_E$-$= b_E$, which we can evaluate from Eq. 2.8 as $\lambda g_{bs}(de_{sat}/dT)/P_a$. Let ΔT be the change in temperature from the original steady value, T-T_0. Eq. 2.26 above becomes

$$\begin{aligned} C_{P,a}\frac{dT}{dt} &= Q^+_{SW,0} + \delta + Q^+_{TIR,0} - Q^-_{TIR,0} \\ &\quad - b_{TIR}\Delta T - Q^+_{E,0} - b_E\Delta T \\ &\quad - Q^-_{c,0} - b_c\Delta T \end{aligned} \tag{2.27}$$

$$\begin{aligned} &= \left(Q^+_{SW,0} + Q^+_{TIR,0} - Q^-_{TIR,0} - Q^-_{E,0} - Q^-_{c,0}\right) \\ &\quad + \delta - (b_{TIR} + b_E + b_c)\Delta T \\ &\quad = \delta - B\Delta T \end{aligned} \tag{2.28}$$

Here, B_{net} is the sum of the derivatives, $b_{TIR} + b_E + b_c$. I ignore here the higher-order terms in $\Delta T$with the second derivatives of the terms with respect to temperature; this is acceptable for a first estimate. The sum of the terms in the first parentheses is clearly zero, representing the initial steady state. We can rewrite this once more, using $(d/dt)\Delta T = (d/dt)T$, so that, dividing by $C_{P,a}$, it has the form

$$\frac{d\Delta T}{dt} = a' - B'\Delta T \tag{2.29}$$

with $a' = \delta/C_{P,a}$ and $B' = B_{net}/C_{P,a}$. This is a simple relaxation equation with the readily-verified solution

$$\Delta T = \frac{a'}{B'}\left(1 - e^{-B't}\right) \tag{2.30}$$

That is, the asymptotic shift in temperature is a'/B', with a characteristic relaxation time $\tau_r = 1/B'$, as the time for the response to reach half its final value. We may make a quick estimate of this time. Table 2.1 presents examples for a thin leaf, 200 µm thick, with a fresh mass per area of 0.2 kg m^{-2}, and a thick cactus phyllode, 20 mm thick. Let the sudden change in absorbed shortwave loading, δ, be 200 W m^{-2}. The estimation of B and then of B' is lengthy; Table 2.1 presents the numerical values of all the terms in the equations, for the environmental conditions specified in the header. The relaxation time is $1/B' = 18.4$ s, quite short for the thin leaves that have very little thermal inertia. The transients in thick phyllodes are correspondingly slower, over 0.7 h. The calculation for phyllodes involves more significant approximations. Their curved surfaces present different angles to incident radiation at different locations. The transport of heat laterally is also more effective than in thin leaves. Accurate calculation of their energy balance requires explicit accounting of space and time, using a partial differential equation. With complex geometry, one must use finite elements.

2. Changes in Temperature After Modifications in Convective Heat Exchange

We can do a similar exercise to estimate the transient response to a change in wind speed. This does not change an energy input directly; rather, it changes the value of g_b, a parameter, not a driving variable such as Q^+_{SW}. All the temperature derivatives of energy terms appear, as in the case presented in the preceding section. The driving term, δ, has a new form, which we see when we formulate the equation for relaxation with a bit more algebra. Letting $g_b \rightarrow g_b' = g_{b,0} + \Delta g_b$, and noting that the leaf temperature changes by an amount ΔT, we may write

$$\begin{aligned}\frac{Q^-_{cc,0}}{C_P} &\rightarrow \left(g_{b,0} + \Delta g_b\right)\left(T_0 + \Delta T - T_{air}\right)\\ &= g_{b,0}(T_0 - T_{air}) + g_{b,0}\Delta T\\ &\quad + \Delta g_b(T_0 - T_{air}) + \Delta g_b \Delta T\\ &= g_{b,0}(T_0 - T_{air})\\ &\quad + \Delta g_b(T_0 - T_{air}) + g_{b,0}\Delta T\end{aligned} \tag{2.31}$$

The first term when grouped with the initial values of the radiative and latent heat terms, makes a sum of zero, because these values are from the initial steady state. The new driving term is $\Delta g_b(T_0\text{-}T_{air})$, which we may denote as δ, as in the previous case. There is a new temperature derivative of the Q_c- term, which is $b_c = C_P g_b$; it includes the contribution of Δg_b. Let us consider the same initial steady state, with the perturbation being a doubling of g_b as the wind increases, changing $C_P g_b$ from 16.7 to 33.4 W m^{-2}. The new δ term is then -16.7 W m^{-2} K^{-1} $\times$ 3 K $=$ -50 W m^{-2} (negative; the leaf is cooled). The new B_{net} term is the same as the value calculated for the case of a change in solar irradiance, except that the contribution of b_c is twice as large. The new value of B_{net} is then 62.9 W m^{-2} K^{-1}. The asymptotic change in leaf T is $\Delta T = \delta/B_{net} = -50/62.9$ K $= -0.8$ K. The relaxation time is somewhat shorter, since B_{net} has increased in magnitude by a factor 62.9/46.1 = 1.36; now this time is 18.4 s/1.36 = 13.5 s.

3. Importance of Temperature Transients for Photosynthesis

The change in temperature with a change in energy-balance terms occurs on a time scale that is short relative to response times of (most) stomata, which are on the order of (sometimes many) minutes (Grantz and Zeiger 1986; Way and Pearcy 2012). On the other hand, it is long with respect to some photosynthetic biochemical responses such as changes in ribulose-1,5-bisphosphate pool size (Pearcy et al. 1997). Although such changes are somewhat buffered by existing metabolite pool sizes, they can still alter photosynthesis in fluctuating environments such as during lightflecks intervened by significant periods in darkness (Pearcy 1988). However, such changes are not included in the steady-state Farquhar et al. (1980) photosynthesis model considered here (Eqs. 2.21 and 2.22). A model that accounts for transients have been advanced by Pearcy et al. (1997).

Changes in the activation of Rubisco enzyme by Rubisco activase are also generally relatively slow (Pearcy et al. 1997 for representative kinetic constants). Perhaps most plants that experience significant excursions in leaf temperature have two different Rubisco activases, one for low T and one for high T, such as has been found in maize (*Zea mays*) (Salvucci and Crafts-Brandner 2004). These change slowly in dominance in the cell, via changes in gene expression over time scales closer to tens of minutes or an hour. This means that a modeler must use the short-term responses of photosynthesis to T, not the long-term responses that include changes in activase expression.

V. Leaves in Canopies

A. General Principles

The principal changes from isolated leaves to leaves in canopies are in radiation interception (shortwave and TIR, both), wind speed, and air temperature and water vapor content. These variations are directly related to the 3-D architecture of leaf (and stem) placement within the canopy (Chap. 8, Evers 2016). There are also correlated changes in leaf properties, such as gradients in leaf photosynthetic capacity with mean light level that varies throughout a canopy (Chap. 4, Niinemets 2016) The net effect of the microenvironmental and physiological variations throughout the canopy is an added level of complexity in computing whole-canopy photosynthesis (Chap. 9, Hikosaka et al. 2016b). The measurement of whole-canopy photosynthesis, such as by eddy covariance (Chap. 10, Kumagai 2016) tests the accuracy of modeling of whole-canopy fluxes of CO_2, water vapor, and sensible heat.

The changes in radiation interception are discussed in the preceding chapter (Chap. 1, Goudriaan 2016). I note that the changes in TIR flux densities are important to model correctly (topmost leaves see as downwelling TIR the relatively "cold" sky-radiated TIR, while leaves deeper in the canopy see more of the "warm" TIR from other leaves, stems, and soil). The changes in wind speed, u, can be modeled with a variety of models, some of them simple (Baldocchi et al. 1983; Goudriaan 1977), commonly as negative exponentials, for the attenuation of u with depth in the canopy expressed as leaf area index (useful only in horizontally uniform layered canopies):

$$u(z) = u(h)e^{a(z/h-1)} \tag{2.32}$$

where h is the top of the canopy, z is the height and the coefficient a can be related to canopy leaf area index, height, and mean leaf spacing (Goudriaan 1977; formulas reported in Campbell and Norman 1998; see also Cescatti and Marcolla 2004).

Atmospheric conditions – air temperature and partial pressures of water vapor and of CO_2 – vary by position within the canopy. In a simple layered canopy, one may average out some variations and regard these scalar variables as functions of a single dimension, depth (Chelle 2005). Basically, the transport of these scalar quantities between layers (and, of course, right to the top of the canopy) is against eddy-diffusive resistances throughout the canopy. There is also an effective resistance of a whole-canopy boundary layer above the canopy, to the height at which one is interested in modeling or measuring fluxes. As a result, the canopy humidifies and heats (or cools) its air under common conditions. This changes the leaf microenvironments (local air T, etc.), at all levels, in turn, changing the leaf fluxes in a feedback loop. Models of the effects have no analytical solutions, so that iterative solutions are needed.

B. Modelling Turbulent Transport and Canopy Profiles of Environmental Drivers

The formulation of the transport resistances for heat and water vapor (and momentum) within and above a plant canopy can be complex. Consider first the transport within the canopy. For laterally uniform canopies that can effectively be regarded as layered, one can resolve layers of finite thickness (finite elements). One attributes to each layer a set of microenvironmental conditions of air temperature, humidity, and CO_2 partial pressure. Each layer then represents a source of the scalar quantities – heat, water vapor, and CO_2 (negative for leaves doing net photosynthesis). Between layers there are resistances, formulated as the reciprocals of eddy diffusivities (Denmead 1964; Denmead and Bradley 1987). Eddy diffusivities are the analog of molecular diffusivities, and they arise from bulk air movement in eddies moving in the air (see Campbell and Norman 1998 for an extensive discussion). There are some simple approximations, such as that the eddy diffusivities of the scalars are all equal to each other, $K_H = K_{wv} = K_{CO_2} = K(z)$, with z = height above the soil, and that $K(z) =$ constant x $u(z)$. Wind speed at the top of the canopy, $z = h$, is impractical to measure, so that one uses wind speed at a reference height above the canopy and then extrapolates it to the top of the canopy, using the standard wind profile

$$u(z) = u_* ln\left(\frac{z-d}{z_m}\right) \quad (2.33)$$

Here, u_* is a friction velocity (effectively a fitting constant), $d \approx 0.65\ h$ is the so-called zero plane displacement (an effective depth within the canopy of a drag sink, at which $u \to 0$), and $z_m \approx 0.1\ h$ is the canopy roughness length. These quantities actually vary with wind speed, because wind distorts the canopies, but the effect is generally considered rather too complex to factor in.

To use this so-called K-theory of transport (Wilson et al. 2003), one relates the concentration of each scalar at a given canopy layer to the concentration of that scalar in the layer below, plus the source strength of the layer below multiplied by the transport resistance between the two layers. The boundary conditions (the magnitudes of the scalars) are only given at the top of the canopy, from measurements at, perhaps, a weather station. One ends up with a series of simultaneous quasi-linear equations. I use the qualifier "quasi" because the sources at one layer affect the microenvironment at the next layer and change its source strength in a nonlinear fashion – that is, transpiration by leaves in any environment is not a linear function of temperature, nor of humidity or CO_2 partial pressure. Iterative solutions are merited.

One can also consider the canopy microenvironment and the canopy resistances as bulked – the microenvironment is uniform inside the canopy, and the canopy resistances to scalar transport are calculated by integrating the eddy diffusivity from the zero-plane displacement height to any chosen reference height, z. The development of the equations is somewhat lengthy, so that I refer to reader to Campbell and Norman (1998). Part of the complexity is that turbulent transport is enhanced if the canopy is liberating sensible heat ($H > 0$) and it is suppressed if the canopy is absorbing sensible heat ($H < 0$). The stability corrections to transport have been formulated using similarity theory, with the following result for the canopy aerodynamic conductance for sensible heat at height z above the canopy $(z > h)$:

$$g_{aH} = \frac{k^2 \rho u(z)}{\left[\ln\left(\frac{z-d}{z_m}\right) + \psi_m\right]\left[\ln\left(\frac{z-d}{z_H}\right) + \psi_H\right]} \quad (2.34)$$

Here, $k = 0.41$ is unitless von Karman's constant, ρ is the molar density of air (mol m^{-3}, when we want g_{aH} in molar units), $z_H = 0.2 z_m$ is the roughness length for heat transport, and the ψ values correct for transport under stable or unstable conditions. Air is stable when it does not spontaneously rise (and by turbulence carry sensible heat upward, $H > 0$); the rate of temperature decrease with height must be less than the rate that would occur by free expansion of air without heat exchange to neighboring air, the adiabatic lapse rate, about 0.098 K per meter (Chapter 4 in Campbell and Norman 1998). The stability correction factors depend upon whether the surface is undergoing net heating or cooling. With net heating ($H > 0$), air parcels near the ground become less dense, making them rise by turbulent transport. The atmosphere is then unstable. With net cooling ($H < 0$), the atmosphere becomes increasingly stratified, or stable. The factors ψ_m and ψ_H have been calculated, partly by theory and partly empirically, as follows:

$$\psi_m = \psi_H = 6\ln(1+\xi) \quad \text{in stable conditions } (H<0) \tag{2.35}$$

$$\psi_H = -2\ln\left[\frac{1+(1+16\xi)}{2}\right]^{\frac{1}{2}},$$
$$\psi_m = 0.6\ \psi_H \quad \text{in unstable conditions } (H>0) \tag{2.36}$$

Here, the stability parameter is

$$\zeta = \frac{z}{L} = -\frac{kgzH}{\rho C_{P,m} T_{air} u_*^3} \tag{2.37}$$

and $C_{P,m}$ is the molar heat capacity of air, g (m s^{-2}) is the acceleration due to gravity, and T_{air}(K) is the air temperature. Because H is involved in the calculation of the resistance (or conductance) for its own generation by the canopy, the solution is iterative, although convergence is not generally problematic. A simpler approximation to the full method above is to use $g_{aH} = Cu$, where the constant C is a function of leaf area index and its vertical distribution (Sellers et al. 1996).

The calculation here applies to reasonably dense, homogeneous canopies. In sparse or non-homogeneous canopies, the theory is only partially developed and partially satisfactory (e.g., Kustas et al. 1994). Even for laterally homogeneous canopies, the theory above applies where the profiles of the scalars are well equilibrated with the surface. If a parcel of air crosses to an area with different vegetation, equilibration to the "new" fluxes from vegetation occurs at a distance ("fetch") that is about 100 times the height above the canopy at which one is measuring the scalar values in the air. At the leading edge of such a change in canopy type, the phenomenon of advection occurs (Klaassen 1992; Raupach 1991; Lee et al. 2004). For example, at the edge of a crop canopy in an arid environment, the incoming air at the leading edge is hot and dry, driving sensible heat influx into the canopy and commonly, higher transpiration than occurs further into the crop along the fetch distance. This is a topic whose quantitative treatment is beyond the scope of this chapter.

This relatively simple K-theory (Wilson et al. 2003) works well in the forward modeling of heat, water vapor, and CO_2 as they diffuse out of the canopy. More sophisticated Lagrangian theories (Raupach 1989; McNaughton and van den Hurk 1995) give very similar results in the forward direction of modeling from leaf or stratum to fluxes, although they give very different results when used in inverse modeling to infer source strengths of heat, water vapor, and CO_2 at different canopy layers (Raupach 1987; Warland and Thurtell 2000).

Other canopy phenomena affect the leaf microenvironments, including cold-air drainage along topographic gradients (Goulden et al. 2006) and sub-canopy blow-through of air beneath the leaf area masses in forests, near the ground where bare trunks are found (Staebler and Fitzjarrald 2004; Vicker et al. 2012). Finally, I note that soil emits fluxes of the scalars, also altering leaf microenvironments. The incorporation of these diverse phenomena into canopy models is an extensive enterprise that is not yet well-covered in the literature. The final pattern of leaf temperature by canopy location and leaf orientation contributes to patterns of leaf and floral development, posing a further important topic for modelers.

In canopies, rain and snow (and dust) get deposited and then redistributed in fairly complex patterns (e.g., Crockford and Richardson 2000), affecting leaf and whole-canopy energy balance as well as photosynthesis and other physiological processes. Modeling the pattern of leaf wetness or snow cover involves a suite of process submodels, for the mechanics of hydrometeor impacts, leaf mechanical responses, and surface flows, including redistribution driven by wind events. The topic is important for boreal forests and rainforests, and I refer interested readers to Gusev and Nasonova (2003) and Niu and Yang (2004).

Figure 2.5 outlines the calculation of energy balance for leaves within a canopy, incorporating the considerations given above, as well as inclusion of the effects of water balance and attendant water stress. Notation for the additional factors involving water is explained in the figure caption. Gutschick and Sheng (2013) present full details for computing radiation penetration statistics from structural information on a canopy composed of a set of trees described by crown positions, sizes, orientations, and foliage density. Other methods are effective for canopies of different structure, such as grasses. Gutschick and Sheng (2013) used simple and possibly novel descriptions of radiation scattered from other leaves and soil to leaves of interest. More accurate radiative-transfer calculations use scattering amplitudes between volume elements (e.g., Sinoquet et al. 2001) or even the individual leaf area elements (e.g., Chelle and Andrieu 1998). The level of computational effort that is merited depends upon the phenomena one wishes to characterize. Simpler methods may suffice for estimation of whole-canopy fluxes for, say, landscape water balance. More detailed methods enable the resolution of microclimates on individual leaves ("phylloclimate"), for studies such as fungal development on leaves (Chelle 2005).

VI. Outlook: Estimation of Large-Scale Fluxes using Leaf Temperature

Leaf temperature enters in a big way in understanding current climate, as well as in predicting future climate. Satellites measure surface temperatures and other variables that can be used to estimate heat fluxes. Atmospheric circulation is driven by the patterns of sensible heat flux, H, and, via conversion of embodied energy to sensible heat as clouds condense, by the latent heat flux, LE. Consequently, estimates of H and LE from satellite measurements inform weather prediction. They also test regional and global climate models, which need verification for their reliability in predicting future climate. Two recent reviews of wide scope on these topics are by Shuttleworth (2007) and by Wang and Dickinson (2012).

Over the land, as opposed to oceans and other bodies of water, leaves cover half the surface area (Myneni et al. 2002), so that knowing leaf temperature is critical. The leaf-to-air temperature difference can be used to compute the sensible heat flux density, H (or, for single leaves, Q_c-), when combined with a knowledge of the boundary-layer conductance. This is readily seen in Eq. 2.16. We may combine the calculation (estimation) of H with estimation of the radiative part of the energy balance in order to estimate latent heat flux, thus, transpiration. Using the more common notation of energy flux densities (W m^{-2}) over scales larger than single leaves, $\lambda E = Q_E$- and $H = Q_c$-, we have $\lambda E =$ (sum of the radiative terms, or net radiation) – H. We then obtain an estimate of λE as a residual in the energy-balance equation. When applying this to a canopy viewed as a single layer, such as viewed by satellite, we must resolve as well the term for conduction of heat into the underlying soil, G. We may write $\lambda E = R_n$

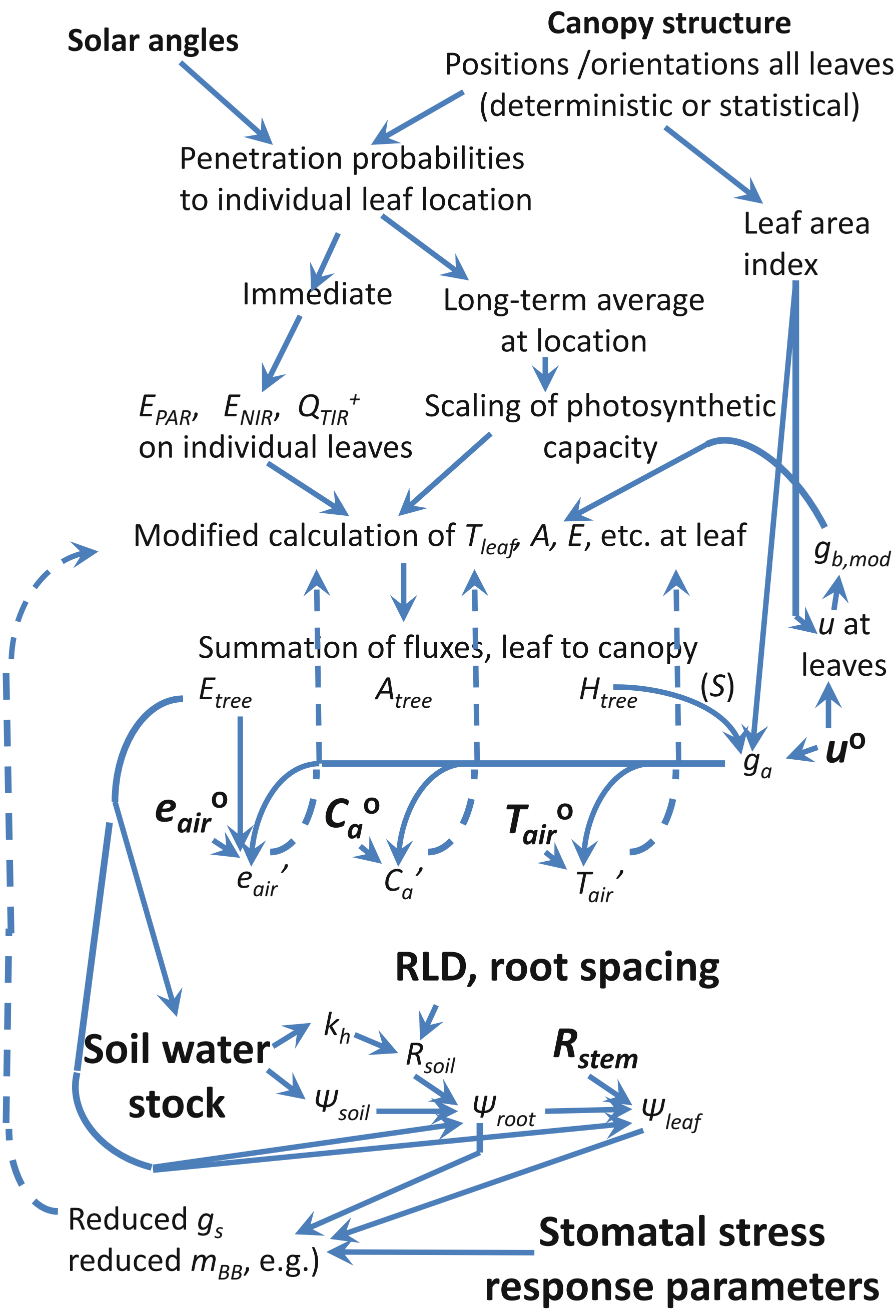

Fig. 2.5. Flowchart for a representative calculation of energy balance and accompanying fluxes of leaves in a canopy. Commonly, the task is calculation of energy balance and fluxes from a representative sample of all leaves on a tree (or other canopy components) in order to compose whole-canopy flux estimates. For a given leaf in the representative sample, the presence of other leaves, stems, and soil affects the propagation of PAR, NIR, and TIR radiation to this leaf. Canopy structure can be described in full for use of a complete radiative transport model, or else statistically using a common turbid medium model (e.g., Gutschick and Sheng 2013). Leaf physiological parameters vary with canopy position; scaling of photosynthetic capacity ($V_{c,\max}^{25}$) often scales with longer-term average PAR irradiance on a leaf (Niinemets 2007), which is computable from radiative transport models run with weather data over a prior time interval. Whole-canopy fluxes (perhaps scaled from individual tree fluxes

– H – G. All the terms, R_n, H, and G may be modeled or may be measured.

The estimation of the radiant fluxes is considered (perhaps with an excess of optimism) as generally accurate. Shortwave energy flux densities are estimated as downwelling SW (using the solar constant 1367 W m^{-2}, with slight variations depending on solar activity) minus the reflected radiation sensed at the satellite. The reflected radiation, of course, arises not only from the surface (canopy and soil) but also from aerosols in the atmosphere. To correct the surface-intercepted radiation for scattering and absorption by aerosols, their content in the atmosphere aerosols must be measured. This is done at very few locations, so that empirical relations are used elsewhere, involving multiple SW wavebands. See, for example, Bastiaanssen et al. (1998). The accounting for varied angles of illumination angles on tilted surfaces is also complex, but possible (Mariotto et al. 2011).

The calculation of H requires that we know the quantity T_{leaf}-T_{air}. Much effort has gone into getting independent, accurate measurements of both temperatures. The air temperature may be taken from ground measurements, or, where these are unavailable, from profiles of air temperature derived by inverse modeling of the TIR fluxes from different atmospheric layers (Strow et al. 2003; King et al. 2003; mathematical background in Twomey 1977; Glasko 1988). Sensing of several different TIR wavebands must be used, each being differentially sensitive to the different temperatures in the layers of the atmosphere. The calculations rely upon small differences in radiative properties of air (really, its water vapor content) at different temperatures, so that the extraction of T_{air} as a function of height in the atmosphere is very sensitive to small errors. It is termed as ill-conditioned in mathematics. Nonetheless, accurate radiative transfer physical theory and mathematical methods such as constrained linear inversion (Twomey 1977) now appear to provide T_{air} near the surface with a root-mean square error cited as slightly below 1 °C (Coll et al. 2009). Before one gets overly optimistic, it is worth noting that an error of 1 °C can lead to notable errors in calculation of H over surfaces with high aerodynamic conductances, g_{aH}, such as tall forests. With g_{aH} = 3 mol m^{-2} s^{-1} in modest wind, the error is g_{aH} multiplied by the heat capacity of air, 29 J mol^{-1} K^{-1} and by the temperature error, or 87 W m^{-2}. This is of the order of H itself in many conditions.

The sensing of leaf temperature itself involves the methods and challenges discussed in the previous Sects. II.D and II.E. A satellite with a wide field of view, say, nearly a radian as with the polar orbiting satellites, will image different parts of the scene at significantly different view angles. This yields different offsets between

Fig. 2.5. (continued) and tree density) alter the in-canopy environment from that of free air conditions measured above the canopy (water vapor and CO_2 contents $e_{air}{}^0$ and $C_a{}^0$ and air temperature $T_{air}{}^0$). Calculation of the in-canopy values (e_{air}, C_a, T_{air}) is iterative. A simple average environment can be calculated from the above-canopy values and the summed canopy fluxes (here, E_{tree} as latent heat flux density, A_{tree} as photosynthetic CO_2 flux density, and H_{tree} as sensible heat flux density) convolved with the aerodynamic conductance of the canopy, g_a (cf. Eq. 2.34 in text). The *arrow* labeled (S) notes application of the stability corrections (Eqs. 2.33, 2.34, 2.35, and 2.36 in text). Dashed arrows indicate propagation of the new computed values for iterative improvement. At bottom is the calculation of soil water fluxes. Mass balance allows calculation of soil water content, hence, hydraulic conductivity k_h and water potential ψ_{soil}. In turn, k_h combined with knowledge of root-length density (*RLD*) and root radius enables calculation of soil-to-root hydraulic conductance, R_{soil}. Then, the product $E_{tree}R_{soil}$ allows calculation of root water potential, ψ_{root}. Whole-tree flux E_{tree} multiplied by stem hydraulic resistance, R_{stem}, allows calculation of leaf water potential, ψ_{leaf}. In several usable models of stomatal responses to water stress, both ψ_{root} and ψ_{leaf} are used along with fixed parameters to calculate a multiplicative factor (<1) applied to conductance, g_s. This factor (*dashed* arrow from *bottom right*) is applied in a new iteration of calculating values of g_s and all leaf fluxes

radiative and kinetic temperatures in different parts of the scene. Variations in view angle also lead to varying corrections for aerosol interference, which can be accounted with some care. A larger problem is that both soil and vegetation are visible at many locations on Earth. Satellites cannot resolve single plants, so that the radiative temperature recorded in a scene element, a pixel, is essentially an algebraic average of the radiative temperatures of the soil and the vegetation (Box 2.3). Problematically, the sensible heat flux is not related simply to any average temperature nor to any average aerodynamic resistance through which soil and vegetation generate sensible heat flux (Box 2.4). It is imperative, then, to find a remedy for this mixing of temperatures. One straightforward method (French et al. 2003) of modest accuracy is to set vegetation temperature equal to air temperature. Then, one solves for soil temperature from the equation relating average radiative temperature to soil and air temperatures and the fractions of soil and vegetation in view (Box 2.3). This approximation does not allow for accurate flux determination when the vegetation is stressed, having reduced transpiration and (unknown) higher temperature.

Box 2.3 Radiative Temperatures Add in a Nonlinear Fashion

The soil and vegetation radiative temperatures combine almost but not quite linearly as an average radiative temperature. The satellite sensor records an energy flux density that it interprets as originating from a blackbody at a uniform radiative temperature, T_{eff}, at a rate per unit area equal to $\sigma T_{eff}{}^4$, where σ is the Stefan-Boltzmann constant. Ignoring the complication of TIR emissivities differing slightly from unity, we may formulate the energy flux density as coming from two sources, one at a temperature T_{veg} that occupies a fraction f_{veg} of the view and another at a temperature T_{soil} occupying a fraction f_{soil} $= 1 - f_{veg}$. Factoring out σ in all the terms, we write

$$T_{eff}^4 = f_{veg} T_{veg}^4 + f_{soil} T_{soil}^4$$

Here, we must use the absolute or Kelvin temperature. We may write $T_{soil} = T_{veg} + \Delta T$. Expanding $T_{soil}{}^4$, we have $T_{veg}^4 = 4T_{veg}^3 \Delta T +$ higher order terms (*h.o.t.*). Taking the fourth root of both sides and using the power series representation that $(a+b)^n = a^n(1 + n[a/b] + n(n\text{-}1)\,[a/b]^2/2 + \ldots)$, we have, by a series of algebraic steps,

$$\begin{aligned}
T_{eff} &= \left[f_{veg}T_{veg}^4 + \left(1-f_{veg}\right)\left(T_{veg}^4 + 4T_{veg}^3\Delta T + h.o.t\right)\right]^{(1/4)} \\
&= \left[T_{veg}^4 + \left(1-f_{veg}\right)\left(4T_{veg}^3\Delta T + h.o.t.\right)\right]^{(1/4)} \\
&= \left(T_{veg}^4\right)^{(1/4)}\left[1 + \frac{1}{4}\left(1-f_{veg}\right)\frac{4T_{veg}^3\Delta T + h.o.t.}{T_{veg}^4} + \ldots\right] \\
&= T_{veg}\left[1 + \left(1-f_{veg}\right)\frac{\left(T_{soil}-T_{veg}\right)}{T_{veg}} + \ldots\right] \\
&= T_{veg}\left[1 + f_{soil}\frac{T_{soil}}{T_{veg}} - \left(1-f_{veg}\right)\frac{T_{veg}}{T_{veg}} + \ldots\right] \\
&= T_{veg}\left[f_{veg} + f_{soil}\frac{T_{soil}}{T_{veg}} + \ldots\right] \\
&= f_{veg}T_{veg} + f_{soil}T_{soil} + \ldots
\end{aligned}$$

The omitted correction terms are tedious to display but have some significance. As a numerical example, consider a the vegetation fraction is 0.3, T_{veg} is 35 °C = 298.2 K, and T_{soil} is 30 °C hotter, as in a hot desert at midday. The linear approximation yields T_{eff} = 0.3*35 + 0.7*65 = 56 °C. The accurate formula yields T_{eff} = 330.0 K = 56.8 °C. The error is of a similar magnitude to the error in air temperature and adds to that error as a statistically independent source. As a more reassuring numerical example, appropriate to temperate farmland with nearly complete canopy closure, take $f_{veg} = 0.8$, $T_{veg} = 28°$, and T_{soil} = 37 °C. The linear approximation yields 29.8 °C, while the accurate formula yields a very similar 29.9 °C.

Box 2.4 Difficulties in Separating Fluxes from Soil and from Vegetation

Vegetation and soil contribute essentially independent fluxes of sensible heat, but through quite different aerodynamic conductances. Again using f_{veg} and f_{soil} as fractional coverages of the land, we may write

$$H = f_{veg} H_{veg} + f_{soil} H_{soil}$$

Here, H_{veg} is the sensible heat flux density (W m^{-2}) over pure vegetation-covered areas, and H_{soil} is that for soil. Each of the two components of H can be written in terms of the molar heat capacity of air, $C_{P,m}$, the aerodynamic conductance above that surface (g_{ver} or g_{soil}), and the temperatures as

$$H = C_{P,m}\left[f_{veg} g_{veg}\left(T_{veg} - T_{air}\right) + f_{soil} g_{soil}\left(T_{soil} - T_{air}\right)\right]$$

We would like to get an expression that uses average temperature, $T_{eff} = f_{veg} T_{veg} + f_{soil} T_{soil}$. This would require that there is a single value of g, but we can't set g_{soil} equal to g_{veg}, as it is often an order of magnitude smaller. We might attempt to define a mean conductance, g_{eff}, evaluating the error terms this introduces:

$$\begin{aligned} H = {} & C_{P,m} g_{eff}\left[f_{veg}\left(T_{veg} - T_{air}\right) + f_{soil}\left(T_{soil} - T_{air}\right)\right. \\ & + C_{P,m}\left[f_{veg}\left(g_{veg} - g_{eff}\right) \times \left(T_{veg} - T_{air}\right) + f_{soil}\left(g_{soil} - g_{eff}\right) \times \left(T_{soil} - T_{air}\right)\right] \end{aligned}$$

The first line above takes a desirable form, as $C_{P,m} g_{eff} [T_{eff} - T_{air}]$. The second line introduces the separate temperatures of soil and vegetation, which we could not estimate from one measurement. The two-source approximation introduced as in the work of French et al. (2003) sets T_{veg} equal to T_{air},. This allows a solution but makes the contribution from vegetation inaccurate.

One longstanding approach is to eliminate surface temperature in the estimation of λE. One can combine Eq. 2.1 for energy balance with Eqs. 2.2, 2.3, 2.7 and 2.15, with extra assumptions about the stomatal and aerodynamic resistances. One obtains the Penman-Monteith equation (Penman 1948; Monteith 1964). To avoid presenting a slew of alternative notation that is more familiar to meteorologists, I offer a summary. One rearranges Eq. 2.1 and coalesces some terms, as done four paragraphs above, writing $\lambda E = R_n - H - G$. All the components of R_n are measurable. The aerodynamic resistance and G are also measurable, though one must know the height of the vegetation to estimate g_{aH}. One also needs the windspeed, commonly by interpolating values from the nearest ground weather stations. The whole land surface is treated as uniform, as a "big leaf." One writes λE as a linear function of temperature, making a linear approximation for the dependence of water vapor partial pressure upon temperature. Critically, the stomatal conductance (used as its inverse, resistance) is set at a fixed, estimated value, acting as a conductance for the whole canopy of vegetation. The result is a linear equation for surface temperature. This temperature is plugged back into the equation for λE, which can then expressed in terms of net radiation R_n, the canopy and aerodynamic resistances, air temperature (for the vapor pressure deficit), and the initial value of water vapor partial pressure at air temperature and its derivative with respect to temperature. The Penman-Monteith equation is used widely in satellite remote sensing, but it has serious limitations. First, soil and vegetation are treated as having the same properties. Applying the equation over sparse vegetation requires elaborate and rather inaccurate corrections. The literature on corrections is quite extensive. Second, it assumes that we have an accurate estimate of stomatal conductance per leaf area. One also needs measurements of leaf area index to scale this up to a whole-canopy conductance, roughly multiplying by sunlit leaf area that varies with solar angle, leaf area index, and leaf angle distribution. However, plant species vary dramatically in stomatal conductance, even under uniform sunlit conditions. Crop species average about threefold higher conductance than wild species (Kelliher et al. 1995). Empirical formulas can be developed for different types of vegetation, as a first correction. Conductance for any given species or genotype is not constant. It varies with photosynthetic rate, thus, with temperature, humidity, light level, etc., as discussed in Sect. III.A. Tellingly, conductance varies with stress, either water stress or nutrient stress. Detection of stress is one major goal of remote sensing, but the Penman-Monteith approach cannot be used for this.

An alternative method has been devised (Bastiaanssen et al. 1998), in which the leaf-to-air temperature difference, $T_{leaf} - T_{air}$ is directly estimated from a calibration scheme. One finds the hottest and coldest pixels in a remotely-sensed scene and identifies these, respectively, as surfaces with $\lambda E = 0$ and $\lambda E = \lambda E_{\max}$, the latter having $H = 0$. The assumption is made, with good justification, that T_L-T_a is linearly related to the radiative temperature alone. Several problems remain. We need an estimate of g_b at the canopy scale, often formulated (Sect. V.B) in terms of surface roughness height, which is a somewhat uncertain small fraction of the height of the vegetation (Rowntree 1988). Vegetation height and leaf area index are the dominant determinants of roughness or of g_b. It is of some help that leaf area index can be estimated with some accuracy from various spectral indices such as the normalized difference vegetation index (Baret and Guyot 1991; Huete et al. 2002; see also Huang et al. 2007). There are numerous improvements on it, as well. However, the only reliable way to estimate vegetation height in a satellite scene is from a knowledge of the plant species in each pixel and their degree of development. There are no useful species identifiers derivable from measurements of surface reflectivity at different wavelengths, despite early optimism (http://ntrs.nasa.gov/archive/nasa/casi.ntrs.nasa.gov/NTRS-PDF/19810020973_1981020973.pdf). This problem is nearly insuperable in many areas of the globe. The estimates are possible in smaller regions with intensive surveys abetted by ground-based studies; a fine example is provided by the Carnegie Airborne Observatory (Asner et al. 2007). A problem shared with Penman-Monteith is that soil and vegetation contributions to fluxes are mixed. Additional problems arise from variation in the angle of illumination over portions of the surface with different slope. Some effective modifications have been offered (Mariotto et al. 2011).

One more problem is intriguing. Over smaller areas of tens to hundreds of meters (sometimes resolved with high-resolution imagery), is that the fluxes H and LE are spatially non-uniform, even for surfaces uniformly covered with vegetation and uniformly lit by the sun. The phenomenon of symmetry breaking is the origin: heated air must rise, just at water heated from below in a pot must rise, but neither fluid can rise as an intact layers. Plumes form at regular or irregular locations, with air sinking in other areas. This structure of Bénard cells (Rayleigh-Bénard convection, see http://en.wikipedia.org/wiki/Rayleigh-Bénard_convection) is readily observed in cooking pots and has been observed on vegetated areas (Cooper et al. 2000; see also Albertson et al. 2001). This means that the differences among pixels at any one time, as in a satellite "snapshot" do not necessarily indicate differences in fluxes on time scales longer than fractions of an hour, after which plume sites shift.

Finally, the interest in estimating λE is heavily in daily-total λE, not instantaneous λE at the time of satellite overpass. Various schemes are used to interpolate LE to all other times of day, often assuming that the evaporative fraction, $\lambda E/(\lambda E + H)$, is constant over the daylight hours (Rowntree 1988). This is moderately crude, as evidenced in ground-base measurements using eddy covariance (Nichols and Cuenca 1993). Modeling of the canopy fluxes could be very helpful in this effort.

VII. Encouragement

Leaf temperature, both in measurement and in theory, involves a wealth of phenomena. It is also a useful variable in many areas of research, extending from photosynthetic physiology to climate change. The problems cited in this chapter are certainly rather numerous but must be viewed as opportunities for research. Collaborations among researchers in plant physiology, biophysics, remote sensing, agronomy, and other fields can surely advance the solutions. Individual researchers can also increase the prospects for progress by mastering fields divergent from their original career experience. It may be little known that Graham Farquhar, who has opened wide areas of research in stable isotopic methods, photosynthetic biochemistry, and more began his career as a nuclear physicist. Some of my own contributions derive some novelty from having begun as a chemical physicist, moving into – perhaps intruding on – fields of plant physiology, ecology, radiative transfer, ecology, and the like. At sufficient intervals, boldness and much work are rewarding.

References

Agristars (1981) http://ntrs.nasa.gov/archive/nasa/casi.ntrs.nasa.gov/NTRS-PDF/19810020973_1981020973.pdf

Alben S, Shelley M, Zhang J (2002) Drag reduction through self-similar bending of a flexible body. Nature 420:479–481

Albertson JD, Katul GG, Wiberg P (2001) Relative importance of local and regional controls on coupled water, carbon, and energy fluxes. Adv Water Resour 24:1103–1118

Anthes RA (1984) Enhancement of convective precipitation by mesoscale variations in vegetative covering in semiarid regions. J Clim Appl Meteorol 23:541–554

Asner GP, Knapp DE, Kennedy-Bowdoin T, Jones MO, Martin RE, Boardman J, Field CB (2007) Carnegie Airborne Observatory: in-flight fusion of hyperspectral imaging and waveform light detection and ranging (wLiDAR) for three-dimensional studies of ecosystems. J Appl Remote Sens 1, 013536. doi:10.1117/1.2794018

Atkin OK, Bruhn D, Hurry VM, Tjoelker MG (2005) The hot and the cold: unraveling the variable response of plant respiration to temperature. Funct Plant Biol 32:87–105

Baldocchi D (1994) An analytical solution for coupled leaf photosynthesis and stomatal conductance models. Tree Physiol 14:1069–1079

Baldocchi DD, Verma SB, Rosenberg NJ (1983) Characteristics of air-flow above and within soybean canopies. Bound Layer Meteorol 25:43–54

Ball JT (1987) Calculations related to gas exchange. In: Zeiger E, Farquhar GD, Cowan IR (eds) Stomatal Function. Stanford University Press, Stanford, pp 445–476

Ball JT, Woodrow IE, Berry JA (1987) A model predicting stomatal conductance and its contribution to the control of photosynthesis under different environmental conditions. In: Biggins JM (ed) Progress in Photosynthesis Research, vol 4. Nijhoff Publishers, Dordrecht, pp 221–224

Ball MC, Egerton JJG, Lutze JL, Gutschick VP, Cunningham RB (2002) Mechanisms of competition: thermal inhibition of tree seedling growth by grass. Oecologia 133:120–130

Barbour MM (2007) Stable oxygen isotope composition of plant tissue: a review. Funct Plant Biol 34:83–94

Baret F, Guyot G (1991) Potentials and limits of vegetation indexes for LAI and APAR assessment. Remote Sens Environ 35:161–173

Bastiaanssen WGM, Menenti M, Feddes RA, Holtslag AAM (1998) A remote sensing surface energy balance algorithm for land (SEBAL) – 1. Formulation. J Hydrol 212:198–212

Bonan GB (2008) Forests and climate change: forcings, feedbacks, and the climate benefits of forests. Science 320:1444–1449

Brutsaert W (1984) Evaporation into the Atmosphere: Theory, History, and Applications. Reidel, Boston

Burden RL, Faires JD (1985) Numerical Analysis, 3rd edn. PWS Publishers, Boston

Campbell GS, Norman JM (1998) An Introduction to Environmental Biophysics, 2nd edn. Springer, New York
Cescatti A, Marcolla B (2004) Drag coefficient and turbulence intensity in conifer canopies. Agric For Meteorol 121:197–206
Chazdon RL, Pearcy RW (1991) The importance of sunflecks for forest understory plants – photosynthetic machinery appears adapted to brief, unpredictable periods of radiation. Bioscience 41:760–766
Chelle M (2005) Phylloclimate or the climate perceived by individual plant organs: what is it? How to model it? What for? New Phytol 166:781–790
Chelle M (2006) Could plant leaves be treated as Lambertian surfaces in dense crop canopies to estimate light absorption? Ecol Model 198:219–228
Chelle M, Andrieu B (1998) The nested radiosity model for the distribution of light within plant canopies. Ecol Model 111:75–91
Chelle M, Renaud C, Delepoulle S, Combes D (2007) Modeling light phylloclimate within growth chambers. In: Prusinkiewicz P (ed) Proceedings of the 5th International Workshop on Functional Structural Plant Models. Napier, New Zealand Print Solutions Hawke's Bay Limited, Napier, pp 571–574
Coll C, Wan ZM, Galve JM (2009) Temperature-based and radiance-based validation of the V5 MODIS land surface temperature product. J Geophys Res Atmos 114, D20102. doi:10.1029/2009JD012038
Collatz GJ, Ball JT, Grivet C, Berry JA (1991) Physiological and environmental regulation of stomatal conductance, photosynthesis and transpiration: a model that includes a laminar boundary layer. Agric For Meteorol 54:107–136
Cooper DI, Eichinger WE, Kao J, Hipps L, Reisner J, Smith S, Schaeffer SM, Williams DG (2000) Spatial and temporal properties of water vapor and latent energy flux over a riparian canopy. Agric For Meteorol 105:161–183
Crockford RH, Richardson DP (2000) Partitioning of rainfall into throughfall, stemflow and interception: effect of forest type, ground cover and climate. Hydrol Proced 14:2903–2920
Dai QD, Sun SF (2006) A generalized layered radiative transfer model in the vegetation canopy. Adv Atmos Sci 23:243–257
Delepoulle S, Renaud C, Chelle M (2009) Genetic algorithms for light sources positioning. In: Plemenos D, Miaoulis G (eds) Proceedings of the 11th 3IA: International Conference on Computer Graphics and Artificial Intelligence. Universite de Limoges, Limoges, p 11
Demmig-Adams B, Adams WW III (2006) Photoprotection in an ecological context: the remarkable complexity of thermal energy dissipation: Tansley review. New Phytol 172:11–21
Denmead OT (1964) Evaporation sources and apparent diffusivities in a forest canopy. J Appl Meteorol 3:383–389
Denmead OT, Bradley EF (1987) On scalar transport in plant canopies. Irrig Sci 8:131–149
Dewar RC (2002) The Ball-Berry-Leuning and Tardieu-Davies stomatal models: synthesis and extension within a spatially aggregated picture of guard cell function. Plant Cell Environ 25:1383–1398
Disney M (2016) Remote sensing of vegetation: potentials, limitations, developments and applications. In: Hikosaka K, Niinemets Ü, Anten N (eds) Canopy Photosynthesis: From Basics to Applications. Springer, Berlin, pp 289–331
Escobedo JF, Gomes EN, Oliveira AP, Soares J (2009) Modeling hourly and daily fractions of UV, PAR and NIR to global solar radiation under various sky conditions at Botucatu, Brazil. Appl Energy 86:299–309
Evers JB (2016) Simulating Crop Growth and Development using Functional-Structural Plant Modeling. In: Hikosaka K, Niinemets Ü, Anten N (eds) Canopy Photosynthesis: From Basics to Applications. Springer, Berlin, pp 219–236
Farquhar GD, Sharkey TD (1982) Stomatal conductance and photosynthesis. Annu Rev Plant Physiol 33:317–345
Farquhar GD, von Caemmerer S, Berry JA (1980) A biochemical model of photosynthetic CO_2 assimilation in leaves of C_3 plants. Planta 149:78–90
French AN, Schmugge TJ, Kustas WP, Brubaker KL, Prueger J (2003) Surface energy fluxes over El Reno, Oklahoma, using high-resolution remotely sensed data. Water Resour Res 39, 1164. doi:10.1029/2002WR001734
Fuentes S, De Bei R, Pech J, Tyerman S (2005) Computational water stress indices obtained from thermal image analysis of grapevine canopies. Irrig Sci 30:523–536
Fuchs M (1990) Infrared measurement of canopy temperature and detection of plant water-stress. Theor Appl Climatol 42:253–261
Gelfan AN, Pomeroy JW, Kuchment LS (2004) Modeling forest cover influences on snow accumulation, sublimation, and melt. J Hydrometeorol 5:785–803
Gershenfeld N (1999) The Nature of Mathematical Modeling. Cambridge University Press, Cambridge, pp 162–166

Glasko VB (1988) Inverse Problems of Mathematical Physics. American Institute of Physics, New York, Transl. of Russian original (1984) by Bincer A

Goudriaan J (1977) Crop Micrometeorology: A Simulation Study. Centre for Agricultural Publishing and Documentation, Wageningen

Goudriaan J (2016) Light Distribution. In: Hikosaka K, Niinemets Ü, Anten N (eds) Canopy Photosynthesis: From Basics to Applications. Springer, Berlin, pp 3–22

Goulden ML, Miller SD, da Rocha HR (2006) Nocturnal cold air drainage and pooling in a tropical forest. J Geophys Res Atmos 111, D08S04. doi:10.1029/2005JD006037

Graham RL (1978) Combinatorial scheduling theory. In: Steen LA (ed) Mathematics Today. Vintage Books, New York, pp 183–211

Granier C, Inze D, Tardieu F (2000) Spatial distribution of cell division rate can be deduced from that of p34(cdc2) kinase activity in maize leaves grown at contrasting temperatures and soil water conditions. Plant Physiol 124:1393–1402

Grantz DA, Zeiger E (1986) Stomatal responses to light and leaf-air water vapor pressure difference show similar kinetics in sugarcane and soybean. Plant Physiol 81:865–868

Greek TJ, Paw U KT, Weathers WW (1989) A comparison of operative temperature estimated by taxidermic mounts and meteorological data. J Therm Biol 14:19–26

Grote R, Monson RK, Niinemets Ü (2013) Leaf-level models of constitutive and stress-driven volatile organic compound emissions. In: Niinemets Ü, Monson RK (eds) Biology, Controls and Models of Tree Volatile Organic Compound Emissions. Springer, Berlin, pp 315–355

Guilioni L, Cellier P, Ruget F, Nicoullaud B, Bonhomme R (2000) A model to estimate the temperature of a maize apex from meteorological data. Agric For Meteorol 100:213–230

Gurevitch J, Schuepp PH (1990) Boundary-layer properties of highly dissected leaves – an investigation using an electrochemical fluid tunnel. Plant Cell Environ 13:783–792

Gusev YM, Nasonova ON (2003) The simulation of heat and water exchange in the boreal spruce forest by the land-surface model SWAP. J Hydrol 280:162–191

Gutschick VP (2007) Plant acclimation to elevated CO_2 – from simple regularities to biogeographic chaos. Ecol Model 200:433–451

Gutschick VP, Pushnik JC, Swanton BA (1988) Use of plant growth chambers at high irradiance levels. Bioscience 38:44–47

Gutschick VP, Sheng Z (2013) Control of atmospheric fluxes from a pecan orchard by physiology, meteorology, and canopy structure: modeling and measurement. Agric Water Manag 129:200–211

Gutschick VP, Simmoneau T (2002) Modelling stomatal conductance of field-grown sunflower under varying soil water status and leaf environment: comparison of three models of response to leaf environment and coupling with an ABA-based model of response to soil drying. Plant Cell Environ 25:1423–1434

Gutschick VP, Wiegel FW (1984) Radiative transfer in plant canopies and other layered media: rapidly solvable exact integral equation not requiring Fourier resolution. J Quant Spectrosc Radiat Transf 31:71–82

Hales K, Neelin JD, Zeng N (2004) Sensitivity of tropical land climate to leaf area index: role of surface conductance versus albedo. J Climate 17:1459–1473

Hanba YT, Moriya A, Kimura K (2004) Effect of leaf surface wetness and wettability on photosynthesis in bean and pea. Plant Cell Environ 27:413–421

Hartmann DL (1994) Global Physical Climatology. Academic, San Diego

Hartz KEH, Rosenørn T, Ferchak SR, Raymond TM, Bilde M, Donahue NM, Pandi SN (2005) Cloud condensation nuclei activation of monoterpene and sesquiterpene secondary organic aerosol. J Geophys Res 110, D14208. doi:10.1029/2004JD005754

Harvell CD, Mitchell CE, Ward JR, Altizer S, Dobson AP, Ostfeld RS, Samuel MD (2002) Ecology – Climate warming and disease risks for terrestrial and marine biota. Science 296:2158–2162

Hikosaka K, Noguchi K, Terashima I (2016a) Modeling leaf gas exchange. In: Hikosaka K, Niinemets Ü, Anten N (eds) Canopy Photosynthesis: From Basics to Applications. Springer, Berlin, pp 61–100

Hikosaka K, Kumagai T, Ito A (2016b) Modeling canopy photosynthesis. In: Hikosaka K, Niinemets Ü, Anten N (eds) Canopy Photosynthesis: From Basics to Applications. Springer, Berlin, pp 239–268

Houghton JT (1977) The Physics of Atmospheres. Cambridge University Press, Cambridge

Huang D, Knyazikhin Y, Dickinson RE, Rautiainen M, Stenberg P, Disney M, Lewis P, …, Myneni RB (2007) Canopy spectral invariants for remote sensing and model applications. Remote Sens Environ 106:106–122

Huete A, Didan K, Miura T, Rodriguez EP, Gao X, Ferreira LG (2002) Overview of the radiometric and biophysical performance of the MODIS vegetation indices. Remote Sens Environ 83:195–213

Idso SB, Reginato RJ, Reicosky DC, Hatfield JL (1981) Determining soil-induced plant water potential depressions in alfalfa by means of infrared thermometry. Agron J 73:826–830

Jackson RD, Kustas WP, Choudhury BJ (1988) A reexamination of the crop water-stress index. Irrig Sci 9:309–317

Jarvis PG, McNaughton KG (1986) Stomatal control of transpiration: scaling up from leaf to region. Adv Ecol Res 15:1–49

Jenkins CLD (1997) The CO_2 concentrating mechanism of C_4 photosynthesis: bundle sheath cell CO_2 concentration and leakage. Aus J Plant Physiol 24:543–547

Johnson IR, Thornley JHM (1984) A model of instantaneous and daily canopy photosynthesis. J Theor Biol 107:531–545

Jones HG, Stoll M, Santos T, de Sousa C, Chaves MM, Grant OM (2002) Use of infrared thermography for monitoring stomatal closure in the field: application to grapevine. J Exp Bot 53:2249–2260

Jones CT, Craig SE, Barnett AB, MacIntyre HL, Cullen JJ (2014) Curvature in models of the photosynthesis-irradiance response. J Phycol 50:341–355

Kavouras IG, Mihalopoulos N, Stephanou EG (1998) Formation of atmospheric particles from organic acids produced by forests. Nature 395:683–686

Kelliher FM, Leuning R, Raupach MR, Schulze E-D (1995) Maximum conductances for evaporation from global vegetation types. Agric For Meteorol 73:1–16

Kimball BA (2005) Theory and performance of an infrared heater for ecosystem warming. Glob Chang Biol 11:2041–2056

Kimes DS, Smith JA, Link LE (1981) Thermal IR exitance model of a plant canopy. Appl Optics 20:623–632

King MD, Menzel WP, Kaufman YJ, Tanre D, Gao BC, Platnick S, Ackerman SA, …, Hubanks PA (2003) Cloud and aerosol properties, precipitable water, and profiles of temperature and water vapor from MODIS. IEEE Trans Geosci Remote Sens 41:442–458

Kirkpatrick S, Gelatt CD Jr, Vecchi MP (1983) Optimization by simulated annealing. Science 220:671–680

Klaassen W (1992) Average fluxes from heterogeneous vegetated regions. Bound Layer Meteorol 58:329–354

Kleczkowski LA, Edwards GE (1991) A low temperature-induced reversible transition between different kinetic forms of maize leaf phosphoenolpyruvate carboxylase. Plant Physiol Biochem 29:9–17

Kogan FN (1997) Global drought watch from space. Bull Am Meteorol Soc 78:621–636

Kreith F (1965) Principles of Heat Transfer. International Textbook Company, Scranton

Kumagai T (2016) Observation and modeling of net ecosystem carbon exchange over canopy. In: Hikosaka K, Niinemets Ü, Anten N (eds) Canopy Photosynthesis: From Basics to Applications. Springer, Berlin, pp 269–287

Kustas WP, Anderson MC, Norman JM (2007) Utility of radiometric-aerodynamic temperature relations for heat flux estimation. Bound Layer Meteorol 122:167–187

Kustas WP, Blanford JH, Stannard DI, Daughtry CST, Nichols WD, Weltz MA (1994) Local energy flux estimates for unstable conditions using variance data in semiarid rangelands. Water Resour Res 30:1351–1361

Lagouarde JP, Kerr YH, Brunet Y (1995) An experimental-study of angular effects on surface-temperature for various plant canopies and bare soils. Agric For Meteorol 77:167–190

Lawrence DM, Thornton PE, Oleson KW, Bonan GB (2006) The partitioning of evapotranspiration into transpiration, soil evaporation, and canopy evaporation in a GCM: impacts on land–atmosphere interaction. J Hydrometeorol 8:862–880

Lee X, Yu Q, Sun X, Liu J, Min Q, Liu Y, Zhang X (2004) Micrometeorological fluxes under the influence of regional and local advection: a revisit. Agric For Meteorol 122:111–124

Leinonen I, Grant OM, Tagliavia CPP, Chaves MM, Jones HG (2006) Estimating stomatal conductance with thermal imagery. Plant Cell Environ 29:1508–1518

Leuning R (1995) A critical appraisal of a combined stomatal-photosynthesis model for C3 plants. Plant Cell Environ 18:339–355

LI-COR Biosciences (2004) Using the LI-6400-XT/ Portable Photosynthesis System. LI-COR Biosciences, Lincoln, NE, USA

Li Z-L, Tang R, Wan Z, Bi Y, Zhou C, Tang B, Yan G, Zhang X (2009) A review of current methodologies for regional evapotranspiration estimation from remotely sensed data. Sensors 9:3801–3853

Liang SL, Strahler AH (1993) An analytical BRDF model of canopy radiative transfer and its inversion. IEEE Trans Geosci Remote Sens 31:1081–1092

Mariotto I, Gutschick VP, Clason DL (2011) Mapping evapotranspiration from ASTER Data through GIS spatial integration of vegetation and terrain features. Photogramm Eng Remote Sens 77:483–493

McCalla TR (1967) Introduction to Numerical Methods and FORTRAN Programming. Wiley, New York

McNaughton KG, Van den Hurk BJJM (1995) A Lagrangian revision of the resistors in the 2-layer model for calculating the energy budget of a plant canopy. Bound Layer Meteorol 74:261–288

Monson RK, Grote R, Niinemets Ü, Schnitzler J-P (2012) Tansley review. Modeling the isoprene emission rate from leaves. New Phytol 195:541–559

Monteith JL (1964) Evaporation and environment. In: The State and Movement of Water in Living Organisms. 19th Symp Soc Exp Biol. Academic, New York, pp 205–234

Murray FW (1967) On the computation of saturation vapor pressure. J Appl Meteorol 6:203–204

Myneni RB, Hoffman S, Knyazikhin Y, Privette JL, Glassy J, Tian Y, Wang Y, . . ., Running SW (2002) Global products of vegetation leaf area and fraction absorbed PAR from year one of MODIS data. Remote Sens Environ 83:214–231

Nichols WE, Cuenca RH (1993) Evaluation of the evaporative fraction for parameterization of the surface energy-balance. Water Resour Res 29:3681–3690

Niinemets Ü (2007) Photosynthesis and resource distribution through plant canopies. Plant Cell Environ 30:1052–1071

Niinemets Ü (2016) Within-canopy variations in functional leaf traits: structural, chemical and ecological controls and diversity of responses. In: Hikosaka K, Niinemets Ü, Anten N (eds) Canopy Photosynthesis: From Basics to Applications. Springer, Berlin, pp 101–141

Niinemets Ü, Diaz-Espejo A, Flexas J, Galmes J, Warren CR (2009) Importance of mesophyll diffusion conductance in estimation of plant photosynthesis in the field. J Exp Bot 60:2271–2282

Niinemets Ü, Keenan TF (2012) Measures of light in studies on light-driven plant plasticity in artificial environments. Front Plant Sci 3:156

Ni-Meister W, Gao HL (2011) Assessing the impacts of vegetation heterogeneity on energy fluxes and snowmelt in boreal forests. J Plant Ecol 4:37–47

Niu G-Y, Yang Z-L (2004) Effects of vegetation canopy processes on snow surface energy and mass balances. J Geophy Res 109, D23111. doi:10.1029/2004JD004884

Parkinson KJ (1985) Porometry. In: Marshall B, Woodward FI (eds) Instrumentation for Environmental Physiology. Cambridge University Press, Cambridge/New York/New Rochelle/Melbourne/Sydney, pp 171–191

Paw U KT (1987) Mathematical analysis of the operative temperature and energy budget. J Therm Biol 12:227–233

Pearcy RW (1988) Photosynthetic utilization of lightflecks by understory plants. Aust J Plant Physiol 15:223–238

Pearcy RW, Gross LJ, He D (1997) An improved dynamic model of photosynthesis for estimation of carbon gain in sunfleck light regimes. Plant Cell Environ 20:411–424

Penman HL (1948) Natural evapotranspiration from open water, bare soil, and grass. Proc R Soc London Ser A 193:120–145

Peñuelas J, Llusià J (2003) BVOCs: plant defense against climate warming? Trends Plant Sci 8:105–109

Räisänen T, Ryyppö A, Kellomäki S (2009) Monoterpene emission of a boreal Scots pine (*Pinus sylvestris* L.) forest. Agric For Meteorol 149:808–819

Raupach MR (1987) A Lagrangian analysis of scalar transfer in vegetation canopies. Q J R Meteorol Soc 113:107–120

Raupach MR (1989) Applying Lagrangian fluid mechanics to infer scalar source distributions from concentration profiles in plant canopies. Agric For Meteorol 47:85–108

Raupach MR (1991) Vegetation-atmosphere interaction in homogeneous and heterogeneous terrain – some implications of mixed-layer dynamics. Vegetatio 91:105–120

Roden JS, Pearcy RW (1993) Effect of leaf flutter on the light environment of poplars. Oecologia 93:201–207

Ross J, Sulev M (2000) Sources of errors in measurements of PAR. Agric For Meteorol 100:103–125

Rowntree PR (1988) Atmospheric parametrization schemes for evaporation over land: basic concepts and climate modeling aspects. In: Schmugge TJ, André J-C (eds) Land Surface Evaporation: Measurement and Parametrization. Springer, New York, pp 5–29

Sage RF, Kubien DS (2007) The temperature response of C_3 and C_4 photosynthesis. Plant Cell Environ 30:1086–1106

Salvucci ME, Crafts-Brandner SJ (2004) Inhibition of photosynthesis by heat stress: the activation state of Rubisco as a limiting factor in photosynthesis. Physiol Plant 120:179–186

Schaepman-Strub G, Schaepman ME, Painter TH, Dangel S, Martonchik JV (2006) Reflectance quantities in optical remote sensing-definitions and case studies. Remote Sens Environ 103:27–42

Schuepp PH (1993) Tansley review No. 59: leaf boundary layers. New Phytol 125:477–507

Segal M, Avissar R, McCumber MC, Pielke RA (1988) Evaluation of vegetation effects on the generation and modification of mesoscale circulations. J Atmos Sci 45:2268–2292

Sellers PJ, Dickinson RE, Randall DA, Betts AK, Hall FG, Berry JA, Collatz GJ, . . ., Henderson-Sellers A (1997) Modeling the exchanges of energy, water, and carbon between continents and the atmosphere. Science 275:502–509

Sellers PJ, Randall DA, Collatz GJ, Field CB, Dazlich DA, Zhang C, Collelo GD, Bounoua L (1996) A revised land surface parametrization (SiB2) for atmospheric GCMs. Part I: model formulation. J Climate 9:676–705

Shuttleworth WJ (2007) Putting the 'vap' into evaporation. Hydrol Earth Syst Sci 11:210–244

Sinoquet H, Le Roux X, Adam B, Ameglio T, Daudet FA (2001) RATP, a model for simulating the spatial distribution of radiation absorption, transpiration and photosynthesis within canopies: application to an isolated tree crown. Plant Cell Environ 24:395–406

Smith JA, Ballard JR, Pedelty JA (1997) Effect of three-dimensional canopy architecture on thermal infrared exitance. Opt Eng 36:3093–3100

Staebler RM, Fitzjarrald DR (2004) Observing subcanopy CO2 advection. Agric For Meteorol 122:139–156

Strow LL, Hannon SE, De Souza-Machado S, Motteler HE, Tobin D (2003) An overview of the AIRS radiative transfer model. IEEE Trans Geosci Remote Sens 41:303–313

Timmermans WJ, Kustas WP, Anderson MC, French AN (2007) An intercomparison of the surface energy balance algorithm for land (SEBAL) and the two-source energy balance (TSEB) modeling schemes. Remote Sens Environ 108:369–384

Tuzet A, Perrier A, Leuning R (2003) A coupled model of stomatal conductance, photosynthesis and transpiration. Plant Cell Environ 26:1097–1116

Twomey S (1977) Introduction to the Mathematics of Inversion in Remote Sensing and Indirect Measurements. Elsevier, Amsterdam, Reprinted by Dover Publications, Mineola, NY, USA

Verstraete MM, Dickinson RE (1986) Modeling surface processes in atmospheric general-circulation models. Ann Geophys Ser B Terres Planet Phys 4:357–364

Vicker D, Irvine J, Martin JG, Law BE (2012) Nocturnal subcanopy flow regimes and missing carbon dioxide. Agric For Meteorol 152:101–108

von Caemmerer S, Furbank RT (2003) The C_4 pathway: an efficient CO_2 pump. Photosynth Res 77:191–207

Wan Z, Zhang Y, Zhang Q, Li ZL (2004) Quality assessment and validation of the MODIS global land surface temperature. Int J Remote Sens 25:261–274

Wang KC, Dickinson RE (2012) A review of global terrestrial evapotranspiration observation, modeling, climatology, and climatic variability. Rev Geophys 10, RG2005. doi:10.1029/2011RG000373

Warland JS, Thurtell GW (2000) A Lagrangian solution to the relationship between a distributed source and concentration profile. Bound Layer Meteorol 96:453–471

Way DA, Pearcy RW (2012) Sunflecks in trees and forests: from photosynthetic physiology to global change biology. Tree Physiol 32:1066–1081

Wilson TB, Norman JM, Bland WL, Kucharik CJ (2003) Evaluation of the importance of Lagrangian canopy turbulence formulations in a soil-plant-atmosphere model. Agric For Meteorol 115:51–69

Wullschleger SD (1993) Biochemical limitations to carbon assimilation in C_3 plants – a retrospective analysis of the A/C_i curves from 109 species. J Exp Bot 44:907–920

Wythers KR, Reich PB, Tjoelker MG, Bolstad PB (2005) Foliar respiration acclimation to temperature and temperature variable Q(10) alter ecosystem carbon balance. Glob Change Biol 11:435–449

Zhang YC, Rossow WB, Lacis AA, Oinas V, Mishchenko MI (2004) Calculation of radiative fluxes from the surface to top of atmosphere based on ISCCP and other global data sets: refinements of the radiative transfer model and the input data. J Geophys Res Atmos 109, D19105. doi:10.1029/2003JD004457